REPORT DOCUMENTATION PAGE

Form Approved
OMB No. 0704-0188

1. REPORT DATE *(DD-MM-YYYY)* 07/31/2008	2. REPORT TYPE Final Technical Report	3. DATES COVERED *(From - To)* April 1, 2006 thru June 30, 2008

4. TITLE AND SUBTITLE Advanced Microwave Ferrite Research (AMFeR): Phase Three	5a. CONTRACT NUMBER
	5b. GRANT NUMBER N00014-06-1-0416
	5c. PROGRAM ELEMENT NUMBER
6. AUTHOR(S) Young, Jeffrey L.	5d. PROJECT NUMBER
	5e. TASK NUMBER
	5f. WORK UNIT NUMBER

7. PERFORMING ORGANIZATION NAME(S) AND ADDRESS(ES) University of Idaho, Office of Sponsored Programs Morrill Hall Room 414 PO Box 443020 Moscow, ID 83844-3020	8. PERFORMING ORGANIZATION REPORT NUMBER

9. SPONSORING/MONITORING AGENCY NAME(S) AND ADDRESS(ES) Office of Naval Research One Liberty Center 875 N. Randolph Street, Suite 1425 Arlington, VA 22203-1995	10. SPONSOR/MONITOR'S ACRONYM(S) ONR
	11. SPONSORING/MONITORING AGENCY REPORT NUMBER PR# 06PR07114-02

12. DISTRIBUTION AVAILABILITY STATEMENT
Unlimited

13. SUPPLEMENTARY NOTES

14. ABSTRACT
Described herein are the key findings and results associated with the Advance Microwave Ferrite Research (AMFeR), Phase III project. The purpose of this research endeavor is to devise ferrite materials for microwave, self-biased circulator applications. The central task of the project is to fabricate ferrites that have a high magnetic saturation, high coercivity and low FMR linewidth. These ferrites are devised for microwave ferrite devices in the context of some integration process.

15. SUBJECT TERMS
Ferrites, circulators, integrated antennas

16. SECURITY CLASSIFICATION OF:			17. LIMITATION OF ABSTRACT UU	18. NUMBER OF PAGES 30	19a. NAME OF RESPONSIBLE PERSON Jeffrey L. Young
a. REPORT U	b. ABSTRACT U	c. THIS PAGE U			19b. TELEPONE NUMBER *(Include area code)* 208-885-6829

Standard Form 298 (Rev. 8-98)
Prescribed by ANSI-Std Z39-18

20080807 178

Final Report

**Advanced Microwave Ferrite Research (AMFeR):
Phase Three**

Dr. Jeffrey L. Young
MRC Institute/Electrical and Computer Engineering
University of Idaho
Moscow, ID 83844-1024
208-885-6829
jyoung@mrc.uidaho.edu

July 31, 2008

Executive Summary:

Described herein are the key findings and results associated with the Advance Microwave Ferrite Research (AMFeR), Phase III project. The purpose of this research endeavor is to devise ferrite materials for microwave, self-biased circulator applications. Materials suitable for this study are the class of M-type, hexagonal ferrites, which typically have large crystalline anisotropies that tend align the magnetic moments of the ferrite in a single direction with the hope of achieving a quasi-saturated state. In addition to having large crystalline anisotropy, the materials must also possess large magnetic coercivities that keep the ferrite saturated even in the presence of a strong, shape-dependent demagnetization field. As a rule of thumb, the coercivity should be of the same strength (or greater) as the magnetic saturation to achieve self-bias operation.

The central task of the project is to fabricate ferrites that have a high magnetic saturation, high coercivity and low FMR linewidth. These ferrites are devised for microwave ferrite devices in the context of some integration process. Past reports for Phase I and II explain several techniques - including liquid phase epitaxy, chemical vapor deposition and sputtering - that have been tried to achieve this end, but have eventually been discarded for various reasons. Such reason include slow deposition growth rates, incompatible material stresses and strains, high FMR linewidths, poor coercivities, etc. The method currently being considered is based on a ferrite and epoxy compound that is hand mixed, compressed and magnetically aligned by external magnets. This method yields lower magnetic saturations (i.e. 2,200 G), but sufficient coercivities that keep the ferrite self-biased. Attempts are currently being made to integrate this compound into a working device. The outcome of this activity will be reported in the Phase IV Final Report.

Concurrent with the material fabrication research is research in the area of wideband, high-isolation circulator design, with particular attention being focused on the integration of a circulator with an antenna. The aim of this research is bring about an integrated assembly that is light-weight, low-profile and small. Two prototype assemblies have been designed, fabricated and tested to prove the soundness of the methodology. Work has also been done on the modeling of electromagnetic waves in ferrites using a finite difference, time-domain methodology. This activity resulted in a high quality simulation of a ferrite phase shifter.

The key team members of this project are divided into two functional groups: Material Science and Microwave Device Design. The Material Science Group, headed by Professors David McIlroy and Wei Jiang Yeh, is responsible for ferrite material fabrication, characterization and validation. The Microwave Device Group, headed by Professor Jeffrey Young, is responsible for device design, fabrication and test. Each group has prepared a report; the reports are attached as appendices. The appendices are organized alphabetically by author as follows:

Appendix A: Wei Jiang Weh and David McIlroy, "Fabrication of Barium Ferrite Disks"
Appendix B: Jeffrey L. Young, "Microwave Circulator Design"

In addition to the key tasks associated with the project, the Microwave Device Group continued its work on the construction of its 2-40 GHz anechoic chamber, 110 GHz probing station and FMR linewidth measurement apparatus. Each of these projects was completed in the middle of Phase Four and will be discussed in that report.

The work performed during Phase III also led to a partnership with Navy SPAWAR, San Diego. Working with J. Rockway, J. Allen and D. Arceo, the team devised an idea of how to use circulators in the design of a comb RF receiver for the Marines. This idea led to the submission of a joint patent application between SPAWAR and the University of Idaho. The idea also led to a three year funded ONR project under the BAA 07-037.

Finally, as a matter of international recognition, Prof. Jeffrey Young was elected to the grade of IEEE Fellow during Phase Three for his work in wave propagation in complex media.

Future Work:

Both the material processes and laboratories are in place to commence with the fabrication of actual self-biased circulators. During Phase Four, both groups will bring their separate skills and knowledge together to design, fabricate and test a microwave, self-biased circulator. At the time of this writing, the two groups have obtained results that look very promising. In fact, by using strontium, bulk ferrite, the Microwave Device Group has fabricated a working self-bias circulator. Further details of these activities will be stated in the Phase Four Final Report.

Journal Publications:

R. S. Adams, B. O'Neil, and J. L. Young, "Integration of microstrip circulators with planar Yagi antennas of several directors," *IEEE Transactions on Antennas and Propagation* (accepted for publication; see attachments).

R. S. Adams, B. O'Neil and J. L. Young, "The circulator and antenna as a single integrated system," *IEEE Antennas and Wireless Propagation Letters* (accepted for publication; see attachments).

R. S. Adams, "A generalized time-stepping algorithm for electromagnetic propagation in ferrite media," *IEEE Transactions on Antennas and Propagation* (accepted for publication; see attachments).

Conference presentations:

W. J. Yeh, A. Abuzir and Y. Kranov, "Barium hexaferrite films made by sputtering and liquid phase epitaxy method for microwave application," *Sixteenth International Conference on Composite and NanoEngineering,* July 2007, Haikou, China.

W. J. Yeh, C. Blengeri-Oyarce, S. Pillamari, J. M. Appikonda, L. Diaz, Y. Kranov and D. McIlroy, "Fabrication of barium ferrite thick films," *10th Annual Meeting of Northwest Section of American Physical Society,* May 2008, Portland, Oregon.

S. Chava, W. J. Yeh and J. Tilles, "Fabrication of metallic nanoporous films," *American Physica Society March Meeting,* March 2008, New Orleans, Louisiana.

W. J. Yeh, S. Chava, J. Tilles, "Metallic nanoporous films fabricated by etching," *9th Annual meeting of Northwest Section of American Physical Society,* May 2007, Pocatello, Idaho.

W. J. Yeh, S. Chava, J. Tilles, "Gold and lead metallic nanoporous films made by etching," at *American Physical Society March Meeting,* March 2007, Denver, Colorado.

R.S. Adams, J.L. Young and B. O'Neil, "Design of microstrip antenna/ferrite circulator systems," IEEE Antennas and Propagation International Symposium, Honolulu, Hawaii, June 2007.

R.S. Adams and J.L. Young, "The finite difference time domain algorithm applied to ferrite media," IEEE Antennas and Propagation International Symposium, Honolulu, Hawaii, June 2007.

Theses and Dissertations:

Benton O'Neil, "Self-biased microstrip Y-junction circulator design using effective cavity models and power ratios," Department of Electrical and Computer Engineering, University of Idaho, Moscow, Idaho, July 2007.

Patents:

J. W. Rockway, J. C. Allen, D. Arceo and J. L. Young, "Broadband Antenna Comb Circulator CLC/CLAC (BA-C4)" (Submitted July 2007).

Appendix A
Fabrication of Barium Ferrite Disks
Wei Jiang Yeh and David N. McIlroy

I. Abstract

During recent years the need for high quality self-biased barium ferrite ($BaFe_{12}O_{19}$) thick films had been increasing due to their chemical stability and oriented hexagonal crystalline structure. Our goal is to fabricate barium ferrite thick disks to be incorporated in self-biased microwave devices. Different methods such as sputtering, pulse laser deposition, chemical vapor deposition and modified liquid phase deposition have been used with limited to no success for thickness above 300μm. Excessive residual stresses of deposited BaM films films and/or low coercivities are the main problems to be solved by this project. We present a low cost solution using $BaFe_{12}O_{19}$ nanopowder mixed with epoxy. The mix is placed on alumina substrates to fabricate 500μm thick disks of BaM to achieve good magnetic properties such as magnetic saturations from 2,000 to 2,500 G and a coercivities fom 3800 to 4000 Oe. In addition, we have integrated these barium ferrite thick disks into microwave devices and successfully deposited copper contact lines for testing and use.

II. Proposal Objective

- Develop barium ferrite thick disks to be incorporated in self-biased microwave devices.
- Integrate the barium ferrite thick disk within the substrate and pattern the metallic traces to achieve a microwave circuit.

III. Methodology

Fabrication of the Barium Ferrite thick film

Each barium ferrite thick disk is made from a combination of commercially available barium ferrite nanopowder (barium dodecairon nonadecaoxide $BaFe_{12}O_{19}$) and 30 minutes epoxy with a ratio of 80/20, respectively. The barium ferrite nanopowder is weighed and placed into the mixing container; the epoxy is then weighed and added to the mix. To help with the mixing process 1 ml of acetone is added to the mix. This first part of the mixing is done for 2 minutes and the goal is to incorporate all the material together to form a dough-like compound, as shown in Figure 1. After that, the dough is mixed by hand for another 2 minutes to achieve a uniform, homogeneous composition; see Figure 2.
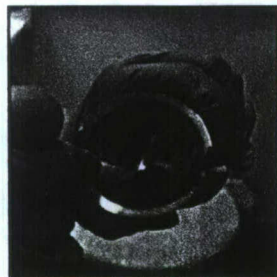
Figure 1. Part one of mixing

Figure 2. Part two of mixing

A small piece of dough is placed in a mechanical press containing one inch magnets. The mixed material is placed in the substrate and carefully pressed, as shown in Figure 3; then another piece of the mixed substance is added on top. The press is closed carefully, as shown in Figure 4. Each press contains two, one inch magnets, with one on top and one on bottom. The function of the magnets is to align the magnetic particles of the mixed substance so that their c-axes are uniformly parallel and oriented. The samples are kept in the high magnetic field for 48 hours, and then released and cured at room temperature for another 48 hours.
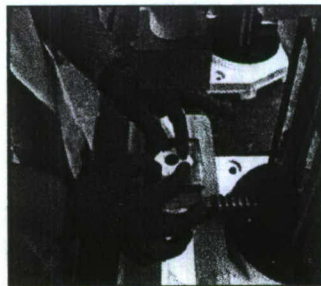

Figure 3. Substrate placed on the press

Figure 4. Sample pressed

Polishing

After the curing process is completed, each sample is polished using a precision lapping/polishing machine (UNIPOL-810), as shown in Figure 5. The polishing process is done in several steps with the lapping machine spinning at 250 rpm:

1. Samples are polished with 320 waterproof sandpaper to remove the excess material.
2. After all the excess material is removed, a polishing cloth is placed in the polishing machine. Three different polishing slurries are sequentially used – 3.0 micron, 0.5 micron and a glass polish 0.05 micron. Each of the slurries is used for 6 minutes for each side.

3. After the polishing is done the samples are place on a hot plate at 45°C for 24 hrs to dry.

Figure 5. Sample being polish

Gap Filling

During the drying step some gaps develop between the ferrite disk and substrate. To remedy this problem an epoxy filler is prepared and placed into the gaps using a thin blade; this particular step requires extreme care. It is important that the epoxy be not applied inside the via holes that are used as part of the electrical circuit. Once all the excess material is removed, the samples are placed again on the hot plate for 24 hrs for curing.

Cleaning and Spin Coating Process

Once the samples are cured, each one is then cleaned with acetone and alcohol using Kimwipes; they are subsequently dried with compressed air. To achieve a uniform surface for copper patterning, each sample is placed in the spin coater KW-4A, shown in Figure 6, and coated with a UV adhesive (Norland Optical Adhesive 68). The spin process lasts about one minute at a rate 4,000 rpm. Samples are then exposed in a $30mW/cm^2$ UV light for 15 minutes and placed on a hot plate at 50°C for 12 hrs. The same process is performed on both sides of the substrate.

Figure 6. Spin Coater KW-4A

Sputtering Process

Sputtering is a technology in which a material is released from a pure material source named target, such Au, Cu, or Ti. The substrate is placed in a vacuum chamber with the target and an inert gas, such as argon, is introduced at low pressure, typically in the range of 10-100mTorr. Gas plasma is created by using a power source, which causes the gas to ionize. The ions are accelerated towards the surface of the target causing atoms of the source material to break off from the target, which then vaporize and condense on all surfaces including the substrate. Difference in pressure and voltage typically relate to the manor in which the ion bombardment of the target is realized. A schematic diagram of a typical DC sputtering system is shown in Figure 7.
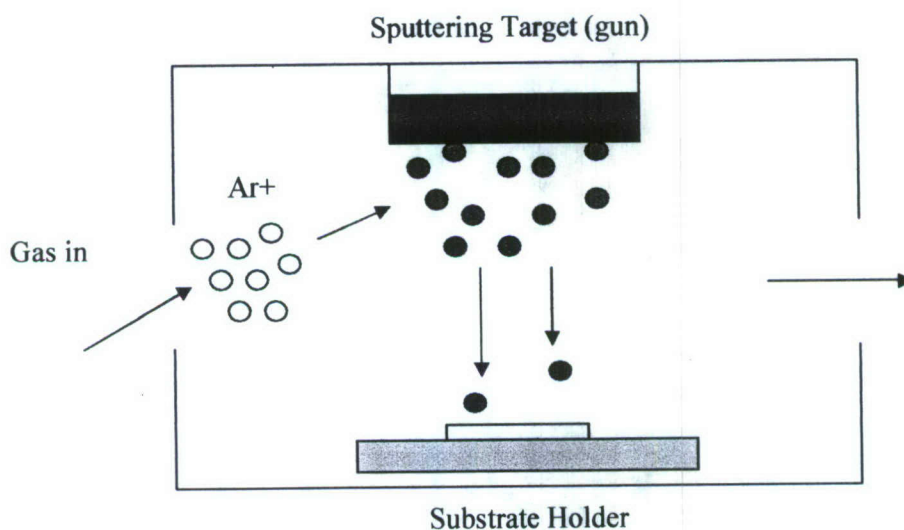

Figue 7. Graphic representation of the sputtering process

We used a single gun sputtering system. Argon DC plasma deposition is used to fabricate all the layers of titanium and copper. The deposition was done at a pressure of 8mTorr

8

with a DC power input of 150W. At these settings, the deposition rate was 0.26μm/min for copper and 500Å/min for titanium.
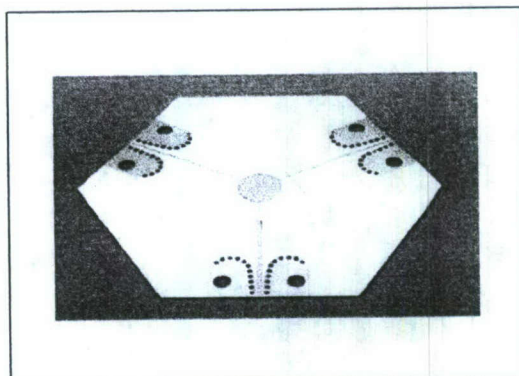

Figure 8. Sample after being sputtered

Measuring Samples

The ferrite samples are characterized using a vibrating sample magnetometer (VSM), as shown in Figure 9. Two measurements are taken: one at 0-degree angle (out of plane) and at 90-degree angle (in plane). Because the hexagonal substrates cannot be placed on the VSM to be measured, circular samples are made at the same time from the same ferrite compound as the original samples. This is shown in Figure 10.
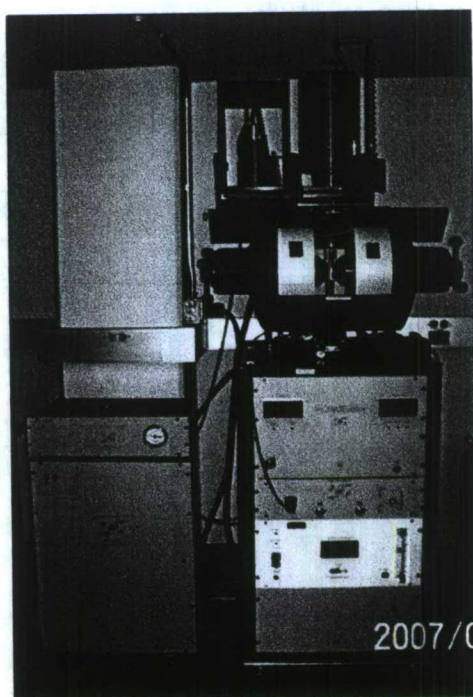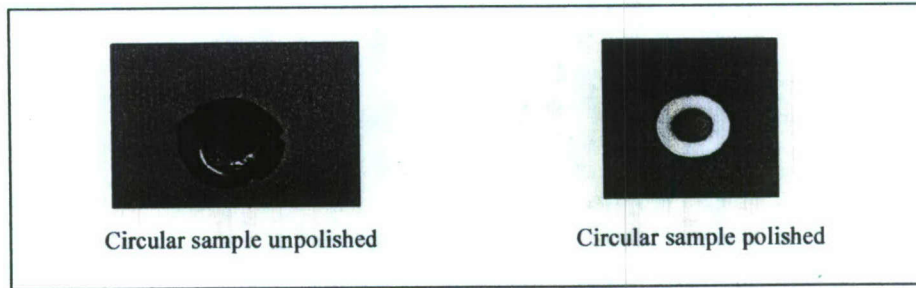

Figure 9. Vibrating Sample Magnetometer

Circular sample unpolished   Circular sample polished

Figure 10. Circular samples to be measure by the VSM

IV. Results

Over the last year different nanopowder/epoxy ratios have been tested. As it can be observed in Graphic 1, the 80/20 ratio has the best overall results. A 90/10 ratio was also tested, but the mixing process was difficult and the uniformity of the compound was compromised. With the 80/20-recipe ratio we obtained very manageable and uniformed material, which resulted in similar and consistent magnetic properties for all samples.

Overall Ratio Effectiveness on VSM Parameters

■ COE ■ 4piMS □ MR ■ SQ
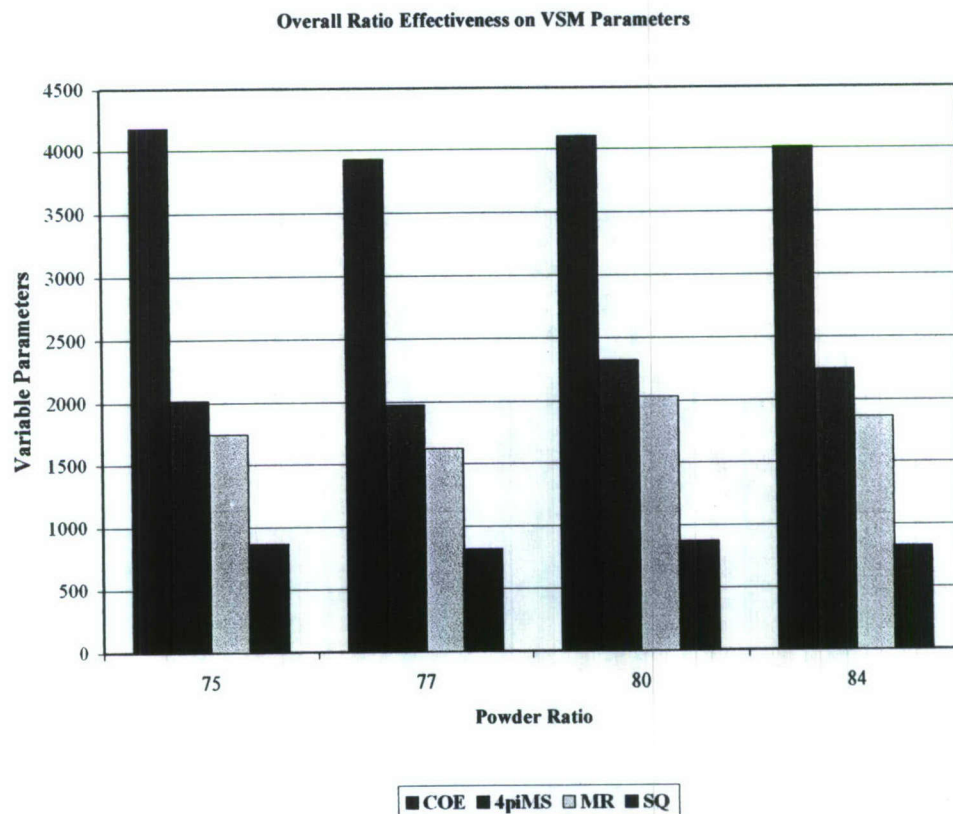
Graphic 1. Recipe ratios tested along with overall outcome of all measure parameters

Different puck thicknesses have also been tested from 0.40 mm to almost 3.00 mm thick. Graphic 2 shows that thicker barium ferrite films tend to have better overall performance.

10

Our objective was to have barium ferrite disks of 0.5 mm in thickness with good magnetic properties. The data confirms that this has been accomplished.

Magnetic Porperties vs. Thickness
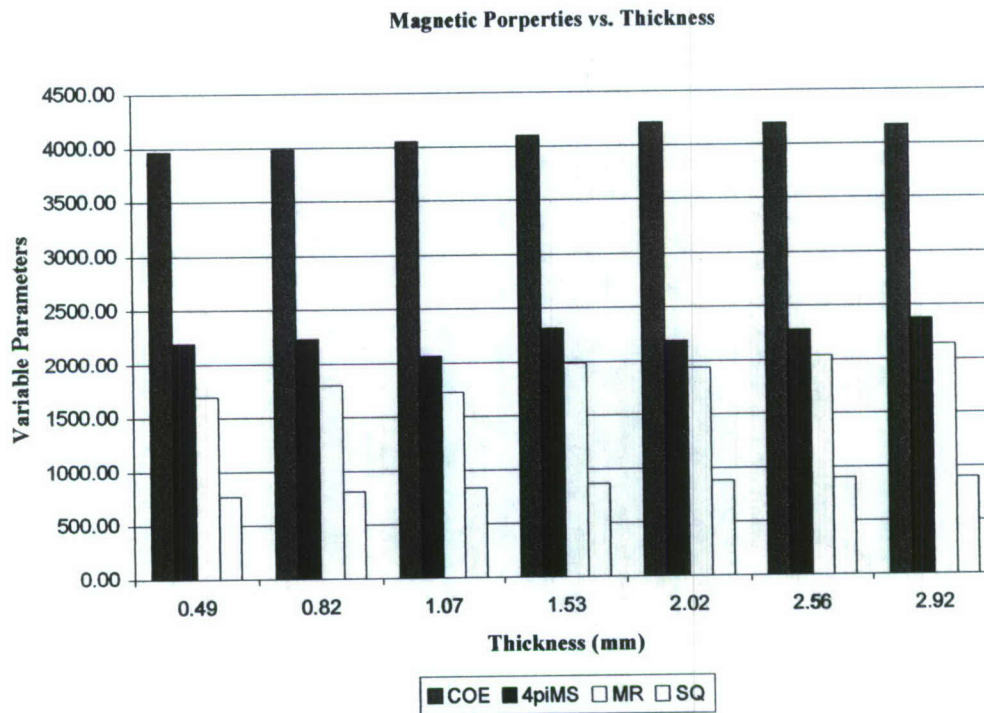
Graphic 2. Different puck thickness and its magnetic properties performance.

Magnetic Properties Measure by the Vibrating Sample Magnetometer (VSM)

Typical measured data obtained by the vibrating sample magnetometer is shown in Figure 11. The most important magnetic properties that we take into consideration for this project are the squareness of the hysteresis loop; the second property is the coercive field that indicates the strength of the magnetic field needed to reduce the magnetization to zero. The third property is the saturation magnetization or $4\pi M_s$, which indicates the maximum possible magnetization of the sample. Lastly the forth property is the remanent magnetization, which indicates the magnetism that remains after a saturating applied field is removed.

In the data shown below, we can observed that the samples presents a squareness of 0.89 S, a coercive field of 4127 Oe, a $4\pi M_s$ of 2,469 Gauss and a remanent magnetization of 2,201Gauss. For self-biased operation, the coercivity should exceed the saturation, which we see is the case. Thus, this sample is a good candidate for a self-biased circulator.
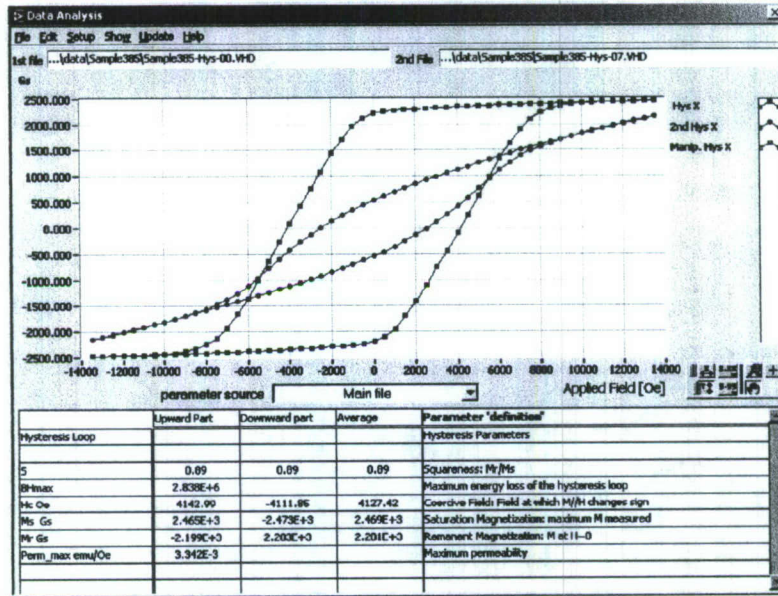
Figure. 11. VSM measurements for the in-plane (red line) and out-of-plane (blue line) hysteresis loops for barium ferrite thick film.

Table 1 shows the results of 200 samples measured by the VSM. Judging by the standard deviation, we can conclude that the technique described herein has high rate of repeatability and consistently produces good thick disks with a squareness average of 0.83 and a coercivity average of 3,986 Oe. Samples also show good values for the saturation magnetization with an average of 2,255 G and 1,862 G for the remanent magnetization.

	Thickness (mm)	Squarness (Sq)	Coercivity Field	Saturation Magnetization (4 π Ms)	Remanent Magnitization (MR)
Mean (μ)	0.76	0.83	3986	2,255	1,862
STDV (σ)	0.24	0.03	296	107	81

Table 1. Value of the mean and standard deviation of 200 samples measured by the VSM

Appendix B

Microwave Circulator Design
Jeffrey L. Young

I. Abstract

During Phase III, a significant portion of the Group's energy was spent on developing techniques for the integration of a microstrip circulator with a planar Yagi antenna to create a compact, light-weight, low-profile integrated subassembly. As reported here, this research activity was very successful with the outcome of building two such, fully-functioning assemblies. Additionally, the team also developed a numerical algorithm that predicts the time-domain wave behavior of a microwave signal within a ferrite. The device that was used for verification of the algorithm was a ferrite phase shifter that exhibited excellent return loss and linear phase characteristics.

II. Proposal Objectives:

The primary objectives for Phase III were:
- To develop a wideband, high isolation, self-biased circulator for microwave signal applications;
- To develop tools and models for the design and development of ferrite devices;
- To integrate ferrite devices with other microwave devices (e.g. antennas) to form a light-weight, low-profile subassembly.

As discussed herein, the last two objectives have been fully realized. As for the first objective, we did not achieve full success until the middle of the fourth phase of the project; this will be reported in the Phase Four Final Report. One of many reasons for this delay was vender-related. A vender that was contracted to fabricate a specialized strontium ferrite and other venders who did tasks like polishing and etching turn what was thought to be a six week process into a six month process.

III. Methodology:

The methodologies and results of the Microwave Device Group are described in the following papers:
- R. S. Adams, B. O'Neil, and J. L. Young, "Integration of microstrip circulators with planar Yagi antennas of several directors."
- R. S. Adams, B. O'Neil and J. L. Young, "The circulator and antenna as a single integrated system."
- R. S. Adams, "A generalized time-stepping algorithm for electromagnetic propagation in ferrite media."

Note: These papers area appended to this report. All three of these papers have been accepted for publication. Unfortunately, attribution to the Phase One contract number was incorrectly cited by the lead author; the research associated with these papers commenced towards the end of Phase Two (but not reported in the Phase Two Final Report) and was carried out throughout Phase Three.

IV. Results

See the aforementioned citations and comments.

V. Future Work

Phase Four is the final phase of the Advanced Microwave Ferrite Research (AMFeR) project. As mentioned in the Executive Summary, a self-biased circulator has been fabricated and tested. The results of those tests clearly indicate that reasonable insertion losses on the order of 1.5 dB and isolations on the order of 15 dB are possible over a narrow band when the device is operating at 22 GHz. The goal of Phase Four is to improve the bandwidths without compromising the insertion and return loss values.

Integration of a Microstrip Circulator with Planar Yagi Antennas of Several Directors

Ryan S. Adams, *Member, IEEE,* Benton O'Neil, *Student Member, IEEE* Jeffrey L. Young, *Senior Member, IEEE,*

Abstract— Two Yagi planar–type antennas are presented that exhibit increased gain and decreased beamwidth in the principle planes when compared with the baseline antenna from the open literature. Two systems are also presented in which each planar antenna is integrated with a ferrite circulator. Excellent pass band characteristics are observed in the experimental and numerical data for both systems. Further, one of the systems is magnetically tuned to provide a superb 30 dB isolation over a bandwidth of 850 MHz. The other system is also magnetically tuned to provide 30 dB isolation over a 300 MHz bandwidth and 40 dB isolation over a 100 MHz bandwidth. Both systems maintain an excellent return loss specification and show improved insertion loss specifications even though the ferrite is tuned to be in partial saturation. Extensive measurement data of the ferrite material and system network parameters are provided to corroborate the claims made herein.

Index Terms— Ferrites, Microwave Circulators, Microstrip Antennas.

INTRODUCTION

A typical monostatic RADAR system consists of a transmitter, receiver, antenna and a circulator, as shown in Figure 1. The design of these systems usually consists of separating the circulator from the remaining components and designing it to some standard interface specification (e.g., 50Ω), as is the adjoining circuitry. Each component is then combined to form the system. Although this approach will yield adequate results, other approaches can provide greater performance and flexibility. We present herein a methodology that considers the design of a planar antenna with a microstrip circulator as a single, integrated component. The antenna topology considered is the planar Yagi–Uda array [1]. To validate the proposed methodology, two integrated antenna/circulator systems are presented.

Simulation data are provided for three substrate antennas: baseline, two director and three director antennas. The baseline antenna is derived from the Yagi–Uda antenna presented by Kaneda et. al. [1]. This antenna exhibits a fairly narrow beamwidth in the E–plane, but the H–plane beamwidth is very wide. The performance of this baseline antenna topology is enhanced through the use of additional director elements that provide a significant improvement in H–plane beamwidth. The directivity of the antenna is also improved as a consequence of the modifications presented herein. When these systems are utilized for communications or RADAR applications, the
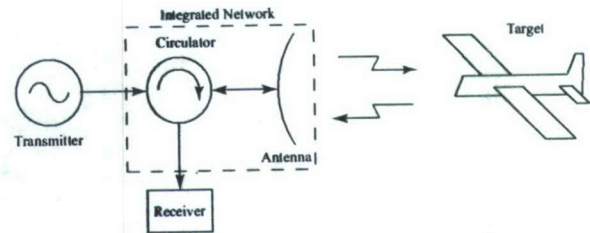
Fig. 1. A monostatic RADAR system.

improved gain compensates for the inherent insertion loss associated with the circulator.

BASELINE ANTENNA

We use as a baseline a modified form of the antenna of Kaneda; modifications were made to account for our choice of substrate thickness (0.5mm) and substrate permittivity (4.5). This antenna topology is shown in Figure 2 and has the following geometrical parameters: $S_{sub} = 1.2$mm, $L_{dir} = 3.3$mm, $W_{dir} = 0.6$mm and $S_{dir} = 2.4$mm. All other geometrical parameters are identical to that of Kaneda, except for minor changes in the miters. This antenna was simulated to determine pattern and impedance information; Figures 3 and 4 show the E–plane and H–plane patterns respectively and Figure 5 shows the input impedance to the antenna. The patterns exhibit the following performance: E–plane beamwidth is 87° with sidelobe levels of 16.5 dB; antenna gain is 5.12 dB; H–plane beamwidth is greater than 180° with no sidelobes. The real part of the input impedance undulates between 25 and 50 Ω in the 12 to 17 GHz band. The imaginary part undulates between 20 and -20 Ω in the same band. Provided that the circulator presents to the antenna an impedance that is close to these values, a good impedance match between the circulator and the antenna can be designed.

This antenna exhibits adequate performance in the Ku-band; however, the H–plane beamwidth is quite broad. To allow tradeoffs in system design, we modify the topology to include additional director elements, which improves H–plane beamwidth as well as antenna gain, as described next.

DOUBLE DIRECTOR ANTENNA

Consider the effect of an additional director element to the geometry of the baseline antenna, as shown in Figure 6. To be consistent with the baseline antenna, we chose the following modified geometrical parameters: $S_{sub} = 1.2$mm, $L_{dir} = 3.3$mm, $W_{dir} = 0.6$mm, $S_{dir} = 2.4$mm and $S_{dir-dir}$
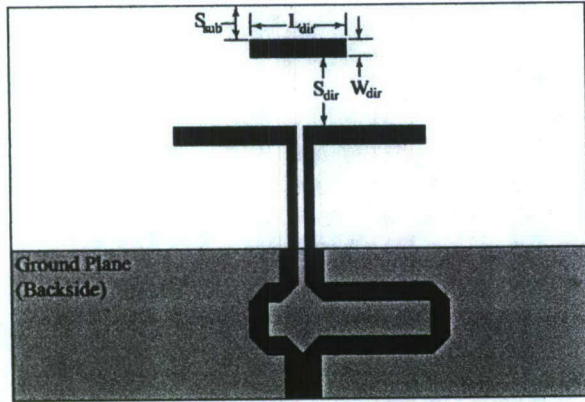
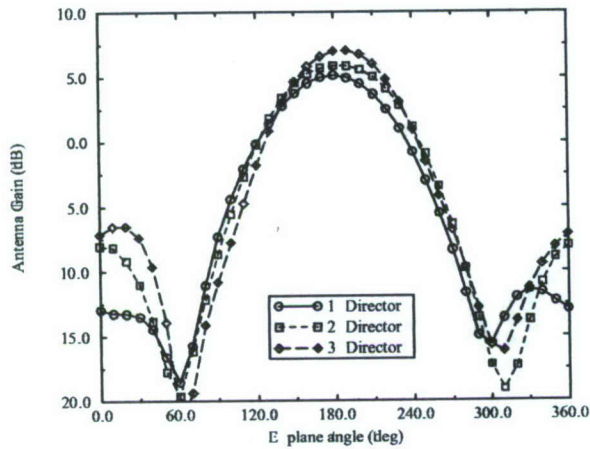Fig. 2. Single director planar Yagi–Uda antenna.

Fig. 3. E–plane pattern comparison for the baseline, double director and triple director antennas.
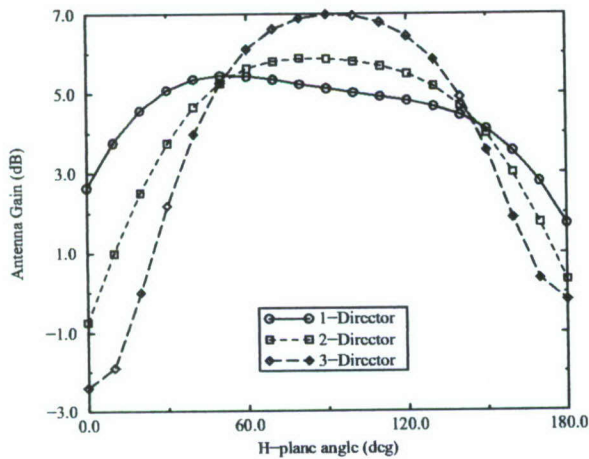

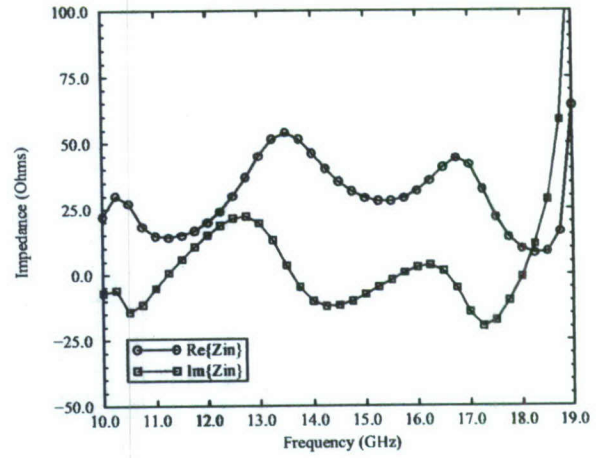Fig. 4. H–plane pattern comparison for the baseline, double director and triple director antennas.

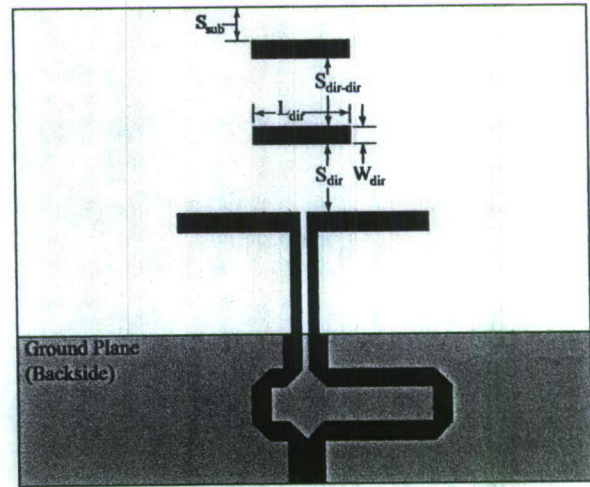Fig. 5. Input impedance of the baseline antenna.

Fig. 6. Double director planar Yagi–Uda antenna.

= 2.4mm. The remaining parameters are identical to those of the baseline antenna. The E–plane and H–plane antenna patterns were simulated with results shown in Figures 3 and 4. From these plots, we note the following: E–plane beamwidth is 93° with sidelobe levels of 13.9 dB; antenna gain is 5.86 dB; H–plane beamwidth is 140° with no sidelobes. The input impedance to this antenna was approximately the same as that of the baseline antenna, and hence the simulated impedance is not shown.

TRIPLE DIRECTOR ANTENNA

The final antenna under consideration uses a third director element to the geometry of Figure 6. Again, we maintain consistency with the previous antennas by choosing the following modified geometrical parameters: S_{sub} = 1.2mm, L_{dir} = 3.3mm, W_{dir} = 0.6mm, S_{dir} = 2.4mm and $S_{dir-dir}$ = 2.4mm. The E–plane and H–plane patterns of this antenna were also simulated and the data are shown in Figures 3 and 4. The following features are noted from these plots: E–plane beamwidth is 76° with sidelobe levels of 13.58 dB; antenna gain is 7.05 dB; H–plane beamwidth is 105° with no

sidelobes. The input impedance of this antenna was also very similar to that of the baseline antenna, and is not shown. This topology yields best overall gain, and narrowest beamwidth in both principle planes, at the expense of slightly higher sidelobe levels.

ANTENNA COMPARISON

With the pattern data of Figures 3 and 4 now known, we have several tradeoffs to consider. First, the baseline antenna is the most compact and has the lowest sidelobe levels; however, it has lower gain and broader H-plane beamwidth. The double and triple director antennas each exhibit improved antenna gain and much narrower beamwidth in the H-plane at the expense of higher sidelobe levels in the E-plane as well as a larger footprint. These tradeoffs can be exploited in overall system design. For example, the insertion loss (which is due to material loss in the ferrite) of a circulator is typically on the order of 0.5-1 dB. An improvement in antenna gain by greater than 1 dB can offset the negative effects of the circulator in the overall system design.

CIRCULATOR DESIGN

To integrate a circulator with the antennas presented previously, the ferrite circuit needs to be described in terms of some network parameters. We do this by appealing to the approach of Bosma [2], who provided the approximate impedance parameters of the ferrite circuit. With this approach, the ferrite region is assumed to be a homogeneous closed cavity with mixed PEC and PMC boundary conditions, and hence a trans-impedance Green's function can be defined as follows [3]:

$$
\begin{aligned}
G(\phi, \phi') = & \frac{Z_f I_0(\gamma_f a)}{2\pi I_0'(\gamma_f a)} \\
& + \frac{Z_f}{2\pi} \sum_{n=1}^{\infty} \frac{I_n(\gamma_f a) e^{jn(\phi-\phi')}}{I_n'(\gamma_f a) + (n\kappa/\mu_f) I_n(\gamma_f a)/(\gamma_f a)} \\
& + \frac{Z_f}{2\pi} \sum_{n=1}^{\infty} \frac{I_n(\gamma_f a) e^{-jn(\phi-\phi')}}{I_n'(\gamma_f a) - (n\kappa/\mu_f) I_n(\gamma_f a)/(\gamma_f a)}. \quad (1)
\end{aligned}
$$

The Green's function relates the vertical electric field on the boundary of the the ferrite to the azimuthal magnetic field on the walls of the ferrite cavity. The appropriate impedance parameters can be determined from these fields with equations similar to

$$
Z_{11} = \int_{(-(\pi/3)-\psi)}^{(-(\pi/3)+\psi)} G(-(\pi/3), \phi') d\phi'. \quad (2)
$$

Although this approach is well-known and extensively used to design circulators, certain errors still exist in the solution. To obtain a more accurate set of network parameters, the geometry must all be simulated via a full-wave electromagnetic solver. However, full-wave solvers take a very long time to arrive at the desired solution when compared with the time required for the Green's function. Hence, a two step process is required: first, the Green's function is repeatedly invoked to find a solution that is approximately correct (say, 20%), and second a full-wave solver is used to validate that
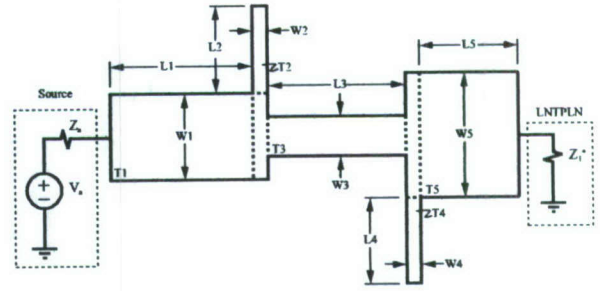

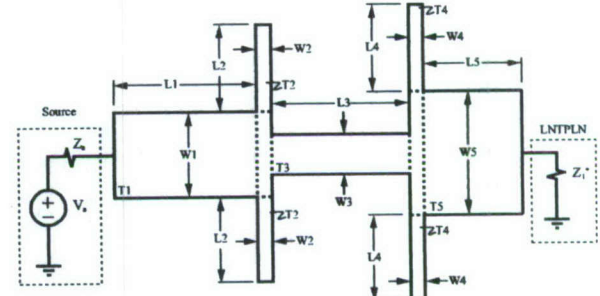Fig. 7. Traditional microstrip impedance equalizer using unbalanced stubs.

Fig. 8. Balanced microstrip impedance equalizer.

the ferrite circuit is adequate, and to generate more accurate network parameters for use in the system integration. Once the network parameters are accurately known, the ferrite region can be regarded as a lossless, nonreciprocal, three-port, linear network (LNTPLN) as presented in [4]. With this network theory representation, the power flow through the network can be evaluated and metrics such as return loss, isolation and insertion loss at each port can be determined. This is described next.

SYSTEM INTEGRATION

To create the integrated components, complex-to-complex impedance equalizers need to be designed to provide the interface between each component of the system to optimize return loss, isolation and insertion loss. This approach of designing the overall system potentially allows for better performance and flexibility than the common approach of isolating each component from the rest of the system and designing each port to match to some standard characteristic impedance, such as 50Ω.

The traditional approach to designing microstrip impedance equalizers consists of a standard topology of alternating through traces and individual stubs, as shown in Figure 7. For most applications, this approach is sufficient. However, when driving an antenna like the ones described previously with an equalizer like that of Figure 7, we note that a field imbalance will occur in the transverse plane of the microstrip as shown in Figure 9. When this signal is presented to the antenna, the balun will be less effective and hence the radiation and input impedance will be affected. Consequently, we have chosen to design our impedance equalizers with electrically balanced stubs as shown in Figure 8.
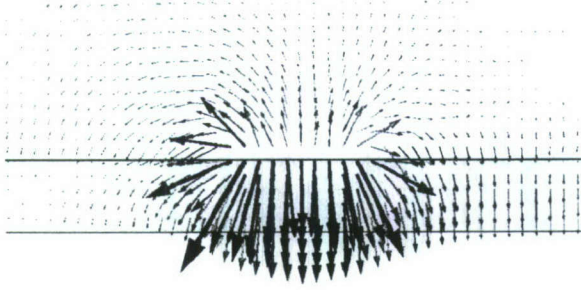
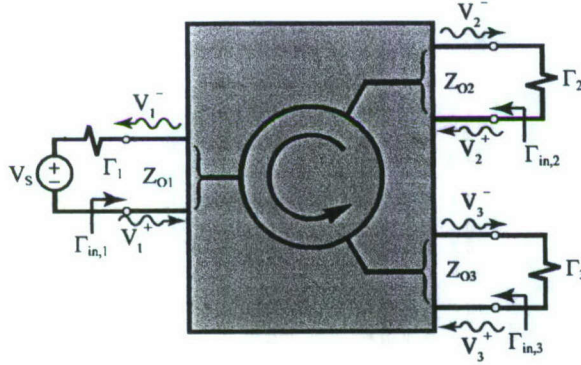Fig. 9. The field structure in the vicinity of an unbalanced stub.

Fig. 10. A block diagram of the antenna/circulator system.

To design the equalizer networks, we follow the approach outlined in [4] with a few modifications. Rather than use the transducer power gain as a metric in conjunction with the circulator impedance, we choose to compute the power flow through the network. For example, we know that two of the equalizers are terminated with a 50Ω, purely real impedance, and the third equalizer is terminated with the impedance function shown in Figure 5. We choose a set of lengths and widths for each of the elements shown in Figure 8 and compute Γ_1, Γ_2 and Γ_3, which are the reflection coefficients that load the circulator at ports 1, 2 and 3, respectively; see Figure 10. Using these reflection coefficients, we can compute the insertion loss at port 1 according to

$$RL_1 = \frac{(1 - |\Gamma_1|^2)(1 - |\Gamma_{in,1}|^2)}{|1 - \Gamma_1\Gamma_{in,1}|^2}, \quad (3)$$

the insertion loss between ports 3 and 1 according to

$$IL_{31} = \left|\frac{V_3^-}{V_1^+}\right|^2 \frac{Z_{o1}}{Z_{o3}} \frac{(1 - |\Gamma_3|^2)(1 - |\Gamma_1|^2)}{|1 - \Gamma_1\Gamma_{in,1}|^2} \quad (4)$$

and the isolation between ports 2 and 1 according to

$$IS_{21} = \left|\frac{V_2^-}{V_1^+}\right|^2 \frac{Z_{o1}}{Z_{o2}} \frac{(1 - |\Gamma_2|^2)(1 - |\Gamma_1|^2)}{|1 - \Gamma_1\Gamma_{in,1}|^2}, \quad (5)$$

where $\Gamma_{in,1}$ is the input reflection coefficient at port 1 of the circulator when ports two and three are loaded with Γ_2 and Γ_3 respectively. Here Z_{o1}, Z_{o2} and Z_{o3} are the port characteristic impedances. We can compute the return loss, insertion loss and isolation for each of the remaining two ports in a similar

manner. We then compare the computed return loss, insertion loss and isolation with the specificied acceptable values. If the computed values satisfy the specification over a broader bandwidth than any previous topology, we keep the design; if not we choose a new set of lengths and widths for the topology of Figure 8 and reiterate.

RESULTS

Two antenna/circulator systems were designed according to the procedure outlined above. Each design utilized a different antenna element as shown in Figures 11 and 12. For each system, impedance equalizers were required for the two ports not interfacing with the antenna to convert from a standard 50 Ω termination to an impedance that optimizes metrics of return loss, isolation and insertion loss. For the circulator/antenna port, the impedance equalizer is one of a complex–to–complex impedance match, where the input impedance of each antenna is modified to optimize these same metrics. We stress that this approach is fundamentally different from designing the circulator and antenna as separate 50 Ω devices.
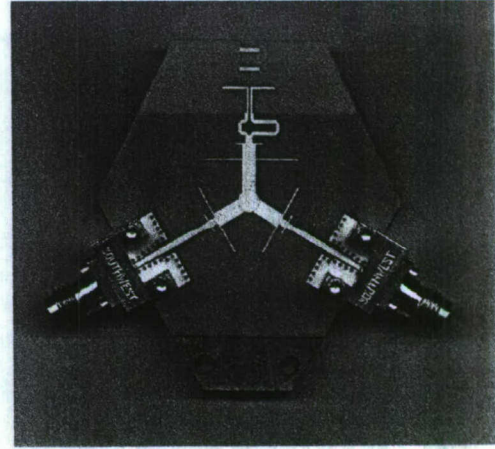

Fig. 11. Circulator/antenna system with two director elements.
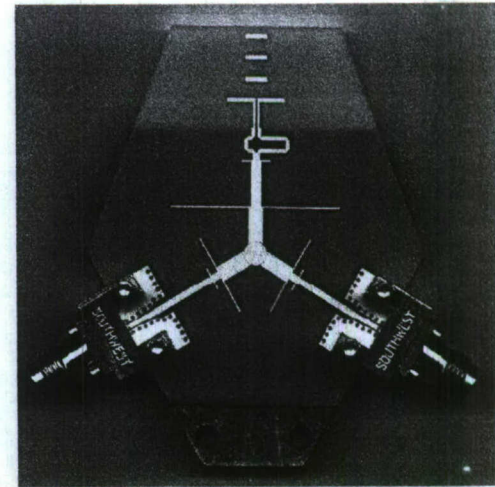

Fig. 12. Circulator/antenna system with three director elements.

The two director system was fabricated on 0.5mm thick Trans–Tech D4 material, which has a dielectric constant of 4.5. The ferrite material selected was Trans–Tech TTI–3000, which has the following properties: $4\pi M_s = 3000$ G, $\epsilon_f = 12.9$, $\tan\delta = .0005$ and radius = 1.75mm. The externally applied field required for these material properties and geometry to assure a zero internal field was set at 2575 Oe. External biasing for this material was provided by a laboratory electromagnet.

The externally measured hysteresis loop for this material is shown in Figure 13, where the "as–designed" bias point of 2575 Oe is shown at the edge of saturation. The peak–to–
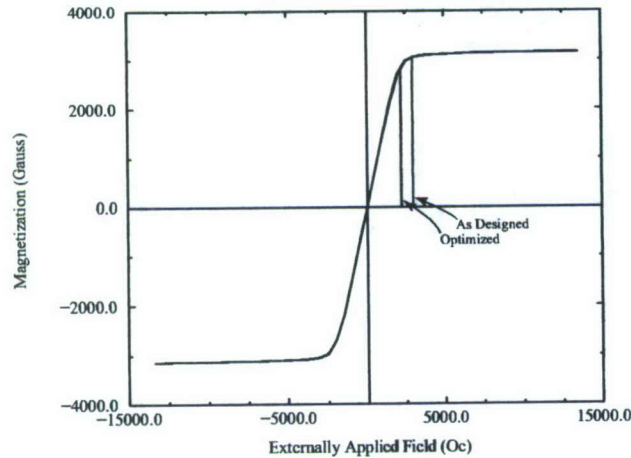

Fig. 13. Measured hysteresis curve of TT1-3000.

peak linewidth of the ferrite material was also measured with results shown in Figure 14. The peak to peak linewidth, at 10 GHz, is 140 Oe, which corresponds to a 3 dB linewidth of 238 Oe. The published linewidth from Trans–Tech is 228 Oe as measured at 9.4 GHz.
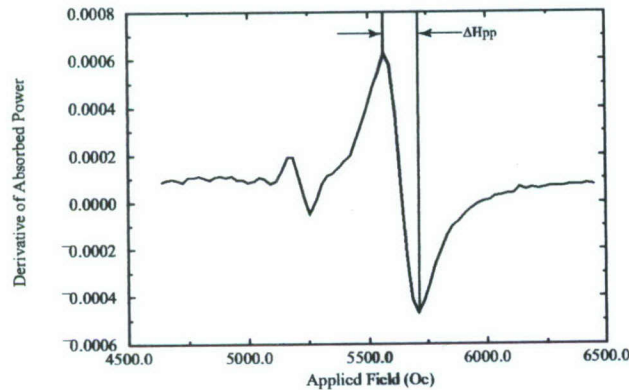

Fig. 14. Measured peak–to–peak linewidth of TT1-3000 at 10 GHz.

The impedance equalizers connected to the two 50Ω ports of the two director system are identical and have the following geometrical parameters: $W_1 = 0.94$mm, $W_2 = 0.216$mm, $L_2 = 1.142$mm, $W_3 = 1.097$mm, $L_3 = 1.067$mm, $W_4 = 0.216$mm, $L_4 = 4.846$mm, $W_5 = 2.255$mm and $L_5 = 4.219$mm. The matching network connecting the circulator to the two–director antenna has the following geometrical parameters: $W_1 =$

1.2mm, $L_1 = 1.201$mm, $W_2 = 0.216$mm, $L_2 = 1.214$mm, $W_3 = 2.196$mm, $L_3 = 2.372$mm, $W_4 = 0.216$mm, $L_4 = 6.983$mm, $W_5 = 2.255$mm and $L_5 = 4.719$mm.

The three director system was also fabricated on 0.5mm thick Trans–Tech D4 material, and the ferrite material was Trans–Tech TTI–3000 with a radius of 1.75mm. Once again, the externally applied bias field was set at 2575 Oe. The matching networks connected to the two 50Ω ports are identical to those of the two–director system. The matching network connecting the circulator to the three–director antenna has the following geometrical parameters: $W_1 = 1.2$mm, $L_1 = 1.101$mm, $W_2 = 0.216$mm, $L_2 = 1.427$mm, $W_3 = 1.561$mm, $L_3 = 6.473$mm, $W_4 = 0.216$mm, $L_4 = 11.47$mm, $W_5 = 2.255$mm and $L_5 = 4.719$mm.

The measured and simulated data for the final fabricated systems are shown in Figures 15 and 16. The measured return loss for each device is about 25 dB; the measured isolation varies from 20 dB to 35 dB across the band of interest. The insertion loss is about 0.8 dB and is quite flat across the band. These measured results correlate quite well to results of simulation. Moreover, we regard isolations and return losses in excess of 20 dB to be quite good and in excess of 25 dB to be superb.
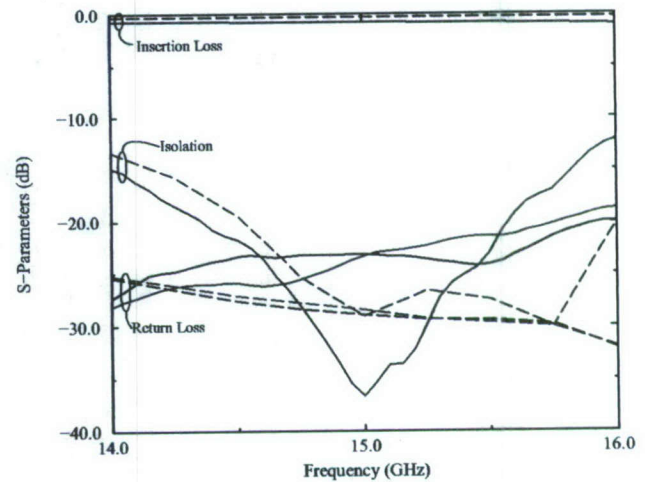

Fig. 15. Measured (solid lines) and simulated (dashed lines) scattering parameters of the two–director element system with a 2575 Oe applied bias.

Although the plots shown in Figures 15 and 16 illustrate the results of the as–designed systems, improved performance may be attained by varying the applied bias field. For example, Figure 17 shows the measured scattering parameters of the two–director antenna system with an applied bias of 2291 Oe rather than that of the previous measurement of 2575 Oe. These tuned parameters exhibit a very good isolation metric of 30 dB over a bandwidth of around 6%. Similarly, Figure 18 shows the measured scattering parameters of the three–director antenna system with an applied bias of 2280 Oe rather than that of the previous measurement of 2575 Oe. These parameters show a very good isolation metric of 30 dB over a relatively narrow bandwidth of 2.1%, and a superb isolation of 40 dB over a narrow bandwidth of 0.8%. Hence by varying the
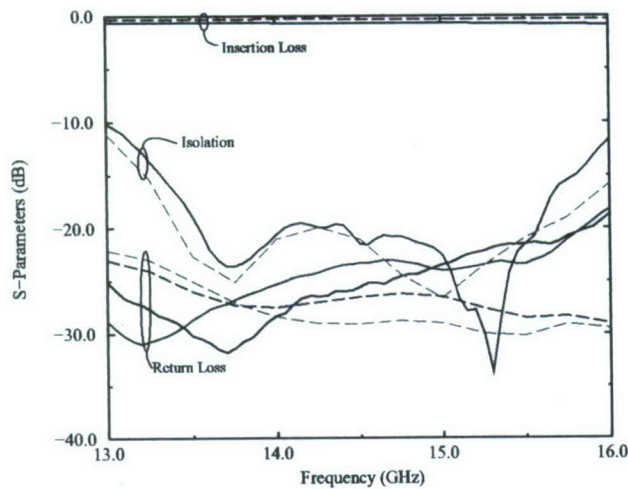
Fig. 16. Measured (solid lines) and simulated (dashed lines) scattering parameters of the three–director element system with a 2575 Oe applied bias.
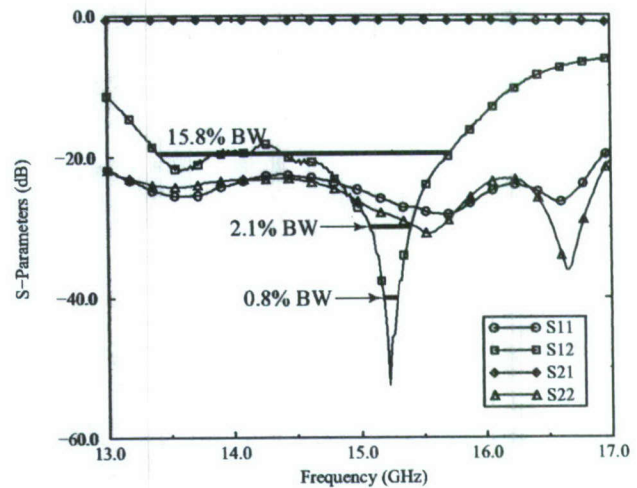

Fig. 18. Measured scattering parameters of the three–director element system with a 2280 Oe applied bias.

applied bias field, we can dynamically optimize these systems for a variety of applications.
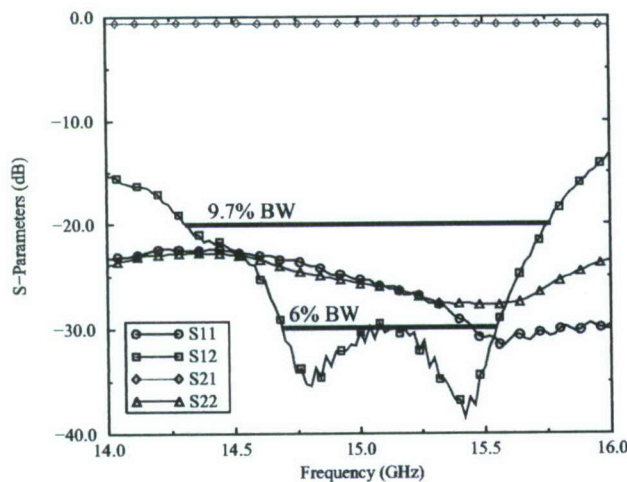

Fig. 17. Measured scattering parameters of the two–director element system with a 2291 Oe applied bias.

The optimized bias point is shown on the measured hysteresis curve of Figure 13, which shows that the material is in a partially saturated state. This partial saturation is significant in light of the commonly held belief that losses increase as the material moves out of saturation. The data shown in Figure 17 and 18 illustrate that this assumption does not always hold, at least for our application. At 15 GHz, for example, the insertion loss changes from 0.8 dB to 0.68 dB for the two director system and from 0.72 dB to 0.68 dB for the three director system. Hence losses have reduced, rather than increased, when the ferrite material is partially saturated.

To illustrate the repeatability of these designs, two circuits were fabricated of each system design. The measurements of each individual circuit showed very good correlation, which points to the insensitivity of the frequency response from device to device.

CONCLUSION

Two Ku–band circulator/antenna systems were presented which exhibit superb performance in the desired frequency spectrum. Each system was magnetically tuned to optimize isolation performance. The two director system realized 6% bandwidth for a 30 dB isolation metric with return loss better than 20 dB. The three director system realized 2.1% bandwidth for a 30 dB isolation metric and 0.8% bandwidth for a 40 dB isolation metric; in both cases the return loss remained better than 20 dB. The measured isolation metric better than 40 dB allows for the design of narrow band simultaneous transmit and receive systems in Ku band.

REFERENCES

[1] N. Kaneda, W. R. Deal, Y. Qian, R. Waterhouse, and T. Itoh, "A broad–band planar quasi–Yagi antenna," *IEEE Trans. Ant. Propagat.*, vol. APS-50, no. 8, pp. 1158–1160, 2002.
[2] H. Bosma, "On stripline Y–circulation at UHF," *IEEE Trans. Microwave Theory Tech.*, vol. MTT-12, no.1, pp. 61–72, 1964.
[3] J. L. Young and J. W. Sterbentz, "The circular, homogeneous–ferrite, microwave circulator: Asymptotic Green's function and impedance analysis," *IEEE Trans. Microwave Theory Tech.*, vol. MTT-51, no. 8, pp. 1939-1945, 2003.
[4] J. L. Young, R. S. Adams, B. O'Neil an C. M. Johnson,"Bandwidth Optimization of an Integrated Microstrip Circulator and Antenna Assembly: Part 1," *IEEE Antennas Propag. Mag.*, vol. 48, no. 6, pp. 47–56, 2006

Ryan S. Adams received from the University of Idaho the BSEE (cum laude) and BS Applied Mathematics degrees (cum laude) in 1999, the MSEE degree in 2005 and the doctoral degree in Electrical Engineering in 2007. He was formerly a graduate research assistant with the department of Electrical and Computer Engineering at the University of Idaho. He is currently serving the Department

of Electrical and Computer Engineering at the University of North Carolina–Charlotte as an Assistant Professor. His research interests include electromagnetic wave propagation in complex media and high frequency circuits. His research awards include third place finalist in the 2007 IEEE Antennas and Propagation International Symposium, Honolulu, Hawaii student paper contest. He is a member of IEEE.

Benton O'Neil received the BSEE degree (cum laude) from the University of Idaho in 2005. He is currently serving the Department of Electrical and Computer Engineering at the University of Idaho as a graduate research assistant. His research interests include computational electromagnetics, high frequency measurement and deembedding techniques.

Jeffrey L. Young received the BSEE degree from Ohio Northern University in 1981 and the MSEE and PhD degrees from the University of Arizona in 1984 and 1989, respectively. He was formerly a doctoral fellow and staff engineer with the Hughes Aircraft Company (1982-1991), Tucson, Arizona. He is currently a Professor of Electrical and Computer Engineering at the University of Idaho (1991-present) and lectures on electromagnetics, antenna theory and design, and microwave circuits. His research interests include electro-optical modulation, ferrite microwave devices, electromagnetic wave propagation in complex media and modern numerical methods in electromagnetics. He served nine years as an editor of the IEEE Antennas and Propagation Magazine and three years as an elected member of the IEEE Antennas and Propagation Society Administrative Committee (2002-2004). He is currently the Antennas and Propagation Society Chapters Coordinator (2004-present) and the General Chair of the 2011 IEEE Antennas and Propagation Society International Symposium and URSI National Radio Science Meeting, Spokane, Washington. In addition to these duties, he has served on numerous Technical Program Committees for the IEEE Antennas and Propagation International Symposium and has chaired several technical sessions at the same. Professor Young is a member of URSI (Commission B), a senior member of IEEE and a registered Professional Engineer in the State of Idaho.

The Circulator and Antenna as a Single Integrated System

Ryan S. Adams, *Member, IEEE*, Benton O'Neil, *Member, IEEE*, Jeffrey L. Young, *Fellow, IEEE*

Abstract—An integration methodology is presented for antenna systems that incorporate a ferrite circulator wherein the geometrical and material parameters of the circulator are adjusted to effect integration; no impedance equalizers are required. To validate the proposed methodology, a system comprised of a microstrip circulator and Yagi planar–type antenna is presented. The overall system exhibits excellent passband characteristics in both the experimental and numerical data. Additionally, the ferrite properties and system network parameters were extensively measured to substantiate the claims made herein.

Index Terms—Ferrites, Microwave Circulators, Microstrip Antennas.

I. INTRODUCTION

When high–performance RADAR or communication systems are designed it is common to break the system into its major components and design each to an interface specification; each component can then be addressed separately from the rest of the system. The interface specification for each component is typically chosen to be a purely real impedance equal to some standardized characteristic impedance (e.g., 50 Ω). This approach simplifies the overall design process, but it does not assure optimality or efficiency of the overall system and typically requires excessive real estate in the final implementation.

In the present work we show that a system that incorporates a circulator (such as a monostatic RADAR system) can be designed without the need for impedance equalization. This task is accomplished by the appropriate selection of geometrical and material parameters to establish the proper characteristic impedances and circulation impedances at each port to naturally interface with the adjoining system components.

To verify the approach herein a system is designed that consists of a circulator and a planar Yagi antenna. We adopt the following notation: port 1 of the circulator is designed to interface with the antenna and ports 2 and 3 are designed to interface with a standard 50 Ω characteristic impedance to allow accurate measurement of system network parameters. The measured system response reveals 25 dB isolation with 14 dB return loss and less than 2.5 dB insertion loss over a bandwidth of 10.5% centered at 9.5 GHz.

Ryan S. Adams is with the Department of Electrical and Computer Engineering, University of North Carolina Charlotte, Charlotte, North Carolina (email: radams41@uncc.edu).

Benton O'Neil and Jeffrey L. Young are with the Department of Electrical and Computer Engineering, University of Idaho, Moscow, Idaho.
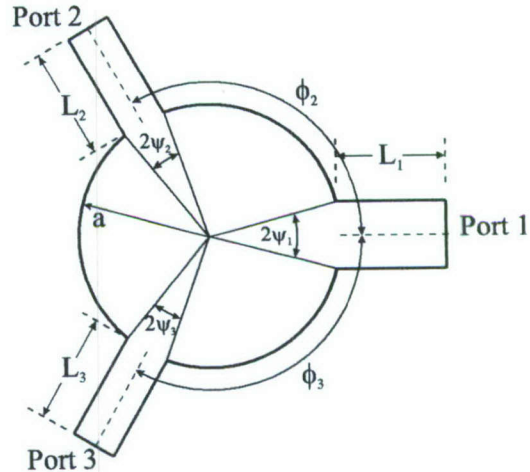

Fig. 1. Geometrical parameters associated with the circulator design.

II. CIRCULATOR MODELING

The intent of this work is to exploit the material and geometrical parameters of a circulator to create an integrated system with desirable circulation and radiation characteristics, without the use of impedance equalizers. A circulator is a three port device that consists of a cylindrical ferrite "puck" with transmission line ports emanating radially outward. The geometrical parameters associated with this device are radius a, coupling angle ψ, thickness h and port angle ϕ, as illustrated in Figure 1. The material parameters are magnetic saturation $4\pi M_s$, effective internal magnetic intensity H_o, ferrite dielectric constant ϵ_f and dielectric constant of the surrounding material ϵ_d.

In traditional circulator design the coupling angles and port angles are chosen to be identical for each port, which assures that the load impedance for perfect circulation, as presented in [1], is identical at each port. When this is the case the trans–impedance Green's function outlined in [2] may be directly employed to determine network parameters of the device. To integrate the circulator with an antenna the Green's function of [2] must be slightly modified to account for non–identical port and coupling angles. For this case the elements of the impedance matrix are given by

$$Z_{ij} = \int_{\phi_j - \psi_j}^{\phi_j + \psi_j} G\left(\phi_i, \phi'\right) d\phi', \qquad (1)$$

where $G\left(\phi_i, \phi'\right)$ is the Green's function of [2]. All nine impedance parameters of the circulator must be computed to

fully characterize the device since the coupling angles and port angles are not rotationally symmetric.

To avoid an abrupt transition in the microstrip trace, each port of the circulator is chosen to equal the width of the feed trace of its corresponding system component. For example, if the width of the feed structure of the component at port 1 equals w_1, then the width of the circulator at port 1 must also equal w_1 and

$$\psi_1 = \sin^{-1}\left(\frac{w_1}{2a}\right). \tag{2}$$

A similar expression is used for ports 2 and 3. This equation clearly shows that the radius of the puck may be varied to effect system design, but the coupling angles of the individual ports may not.

The load impedances seen by each port of the circulator may be complex and frequency dependent, so the interconnecting microstrip lengths may contribute to a broadband response. For this reason L_1, L_2 and L_3 of Figure 1 are included as variables in the design process.

III. DESIGN APPROACH

The system integration procedure begins with a full characterization of the components that will connect to the circulator. This characterization can be accomplished with a full–wave solver, measurement, or existing model. To assure a valid characterization, all components must incorporate a common substrate dielectric constant and thickness. Additionally, each component must have a well defined input microstrip trace geometry that will remain constant throughout the process.

To complete the system integration procedure, the Green's function is employed as described previously to choose appropriate values of microstrip interconnecting trace lengths L_1, L_2, L_3, radius a, port angle ϕ_2, ϕ_3 and saturation magnetization $4\pi M_s$; these parameters are shown in the diagram of Figure 1. The Green's function is invoked in connection with an appropriate optimization procedure to determine an acceptable system response.

For this integration approach we have chosen to employ a multi–objective optimization procedure based on the standard circulator metrics of return loss, insertion loss and isolation. With the load reflection coefficients given by Γ_i, $i = 1, 2, 3$, the return loss at port i is given by

$$RL_i = \frac{\left(1 - |\Gamma_i|^2\right)\left(1 - |\Gamma_{in,i}|^2\right)}{|1 - \Gamma_i\Gamma_{in,i}|^2}, \tag{3}$$

and the power delivered to port i from port j is given by

$$P_{ij} = \left|\frac{V_i^-}{V_j^+}\right| \frac{Z_{oj}}{Z_{oi}} \frac{\left(1 - |\Gamma_i|^2\right)\left(1 - |\Gamma_j|^2\right)}{|1 - \Gamma_j\Gamma_{in,j}|^2}. \tag{4}$$

In each of these equations, $\Gamma_{in,i}$ is the input reflection coefficient at port i of the circulator when the remaining ports are loaded with their respective reflection coefficients, Z_{oi} is the port characteristic impedance of the ith port and V_i is the voltage at port i when each port is loaded with its respective reflection coefficient.

It should be noted that the Green's function provides a good design tool, as it is computationally robust, but the results
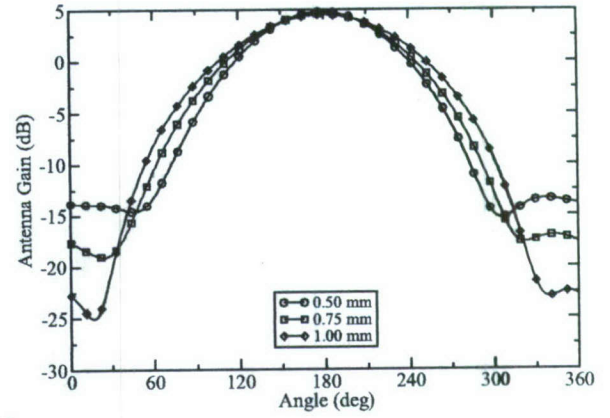

Fig. 2. Simulated E–plane antenna patterns of the antenna of [3] with various substrate thicknesses.

are approximate. Consequently, exclusive use of the Green's function for system design will create a design that operates near the desired value, but may not meet specifications. Further design modifications may be required with a full–wave solver prior to fabrication.

IV. RESULTS

A system comprised of a ferrite circulator and planar antenna was designed and fabricated following the theory presented above. The antenna was chosen to interface to port 1 of the circulator; ports 2 and 3 were designed to interface to a standard 50 Ω characteristic impedance to aid in accurate network parameter measurement. The substrate material used in this system design was USTC995 by US Technical Ceramics, which has a dielectric constant of $\epsilon_d = 9.6$ and $\tan\delta = 0.0007$.

The antenna element was chosen from among three options based on the planar Yagi antenna of Kaneda [3]; modifications were made in the substrate thickness, dielectric constant ($\epsilon_d = 9.6$) and minor changes in the miters. The substantive difference between the three antennas was the choice of dielectric thickness; values of 0.5 mm, 0.75 mm and 1.0 mm were investigated. The antenna with each substrate thickness was simulated using Ansoft's HFSS to determine pattern and impedance data. Figures 2 and 3 show the E–plane and H–plane antenna patterns, respectively, and Figure 4 shows the input impedance values of each antenna. The trace width of the antenna feed line in all cases was fixed at 1.2mm, which also became the width of port 1 of the circulator.

The optimum criteria for the choice of antenna was a flat impedance response, with approximately zero imaginary part near 10 GHz, as this response was believed to be easily matchable with a circulator at that frequency. In addition to this impedance criteria, it was desired that the antenna pattern exhibit a large main beam with low sidelobes in both principal planes. The antenna with 0.75mm dielectric was chosen for integration, since it exhibited better than 20dB side lobe levels and the best impedance response of the available choices. This choice of dielectric constant and thickness corresponds to a 50
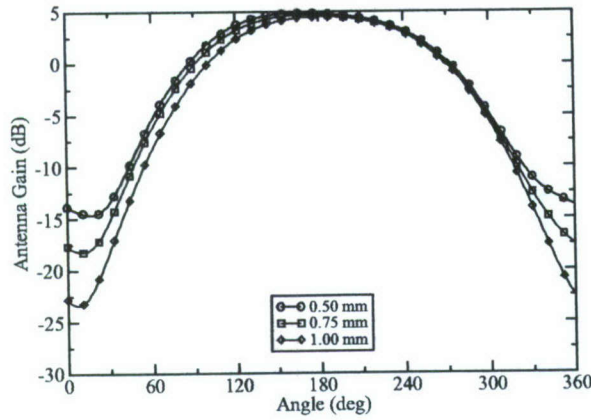
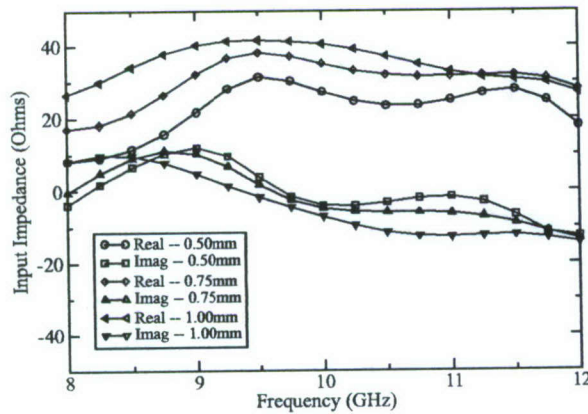Fig. 3.   Simulated H–plane antenna patterns of the antenna of [3] with various substrate thicknesses.

Fig. 4.   Simulated input impedance of the antenna of [3] with a substrate thickness of 0.75mm.
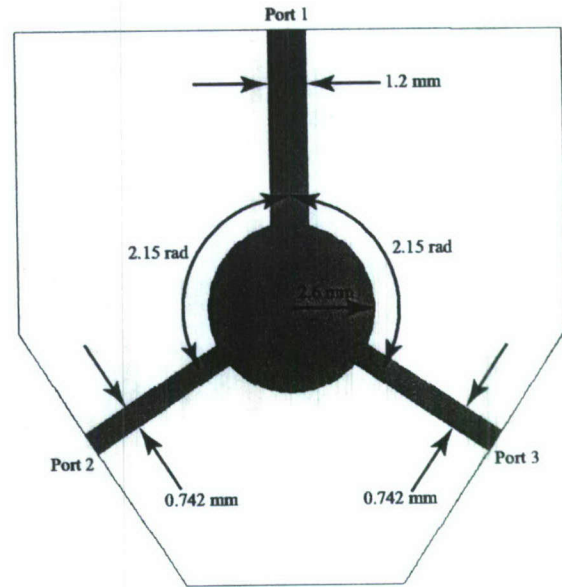

Fig. 5.   Puck design used with the 0.75mm thickness antenna connected to port 1.
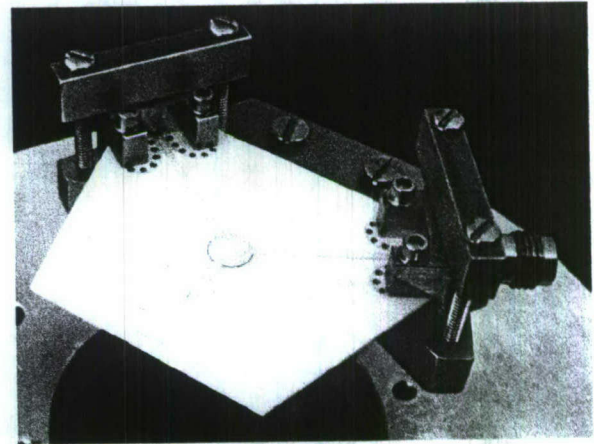

Fig. 6.   Overall system comprised of the ferrite puck of Figure 5 and the antenna of [3] with a 0.75mm thick dielectric.

Ω microstrip line width of 0.742mm, which defined the widths of ports 2 and 3 of the circulator.

The resulting circulator design is shown in Figure 5, and the fabricated system is shown in Figure 6. The geometrical parameters for the circulator were found to be $a = 2.6$mm, $h = 0.75$mm, $\psi_1 = 0.233$ rad, $\psi_2 = \psi_3 = 0.14$ rad, $\theta_2 = 2.15$ rad, $\theta_3 = -2.15$ rad and $L_1 = 2.9$mm. In this design, L_2 and L_3 were arbitrarily chosen since ports 2 and 3 were loaded with their respective characteristic impedances. For the test circuit shown in Figure 6, $L_2 = L_3 = 20$mm as measured from the edge of the dielectric to the edge of the puck. The ferrite material chosen for this system was Trans–Tech TT1-1000 with material parameters $4\pi M_s = 1000$ Gauss, $\epsilon_f = 11.6$ and $\tan \delta_f = 0.00025$.

The ferrite hysteresis and ferromagnetic resonance properties were measured, with results shown in Figures 7 and 8, respectively. The hysteresis curve demonstrates that although the material exhibits a saturated magnetization of 1000 Gauss, the magnetization at the bias point is approximately 900 Gauss–a reduction of 10% from full saturation. Additionally, the peak–to–peak linewidth of the material was measured at 10.0 GHz to be 103 Oe which corresponds to half power linewidth of 179 Oe. As will be seen in the ensuing simulation

data this linewidth value leads to moderately low insertion losses.

Comparison of the simulated and measured response is shown in Figures 9 and 10. These figures clearly illustrate a circulating response, with a return loss above 14 dB, insertion loss below 2.5 dB and superb isolation better than 25 dB over the band from 9–10 GHz. Certain deviations from simulation are apparent particularly in the insertion loss measurement which was simulated to be in the vicinity of 0.5 dB. First, the higher than expected insertion loss is linked to the coax to microstrip transitions and fabrication deficiencies. Simulation of the circuit with transitions versus without showed approximately 1dB insertion loss directly associated with the use of these transitions. Second, the porosity of the alumina substrate sample required that a very thin metal layer be used to form the transmission lines. Third, small gaps existed at the
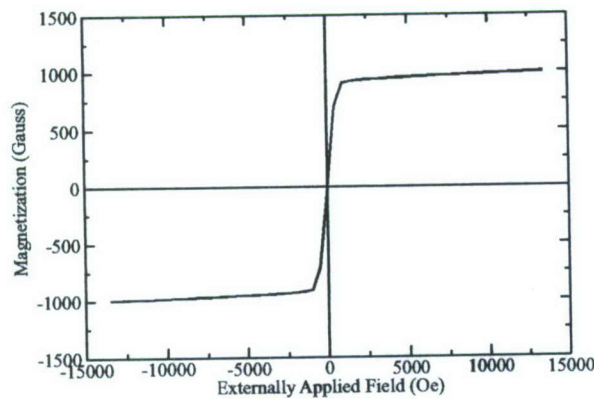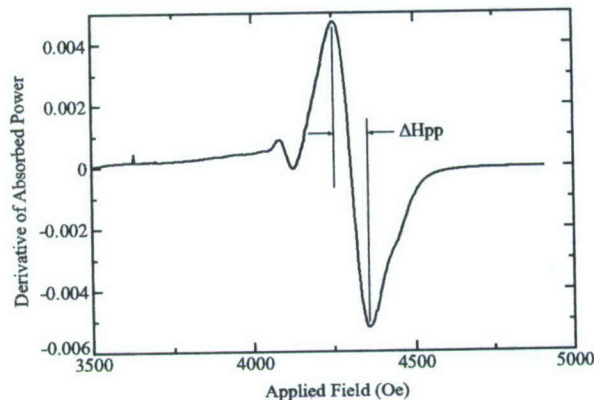
Fig. 7. Measured hysteresis curve of TT1-1000.

Fig. 8. Measured peak–to–peak linewidth of TT1-1000 at 10 GHz.

Fig. 10. Simulation and measurement insertion loss and isolation of the system of Figure 6.

ferrite/dielectric boundary which, coupled with the thin metal layer, created small gaps in the feed traces at the boundary of the circulator. Fourth, the quasi-saturated state of the ferrite per Figure 7 is known to affect loss. Our model assumes a fully saturated ferrite.

V. CONCLUSION

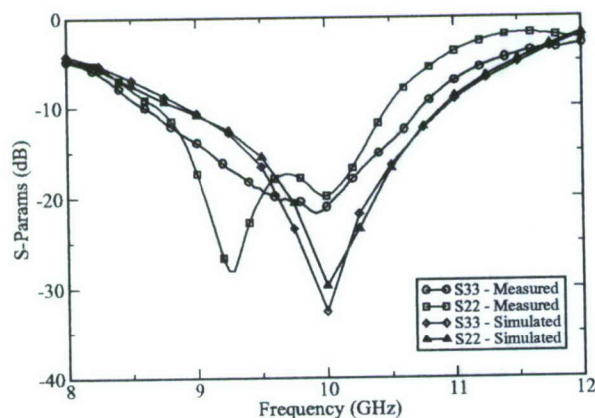A novel design procedure has been devised for antenna systems that incorporate a ferrite circulator. The procedure utilizes the inherent material and geometrical parameters of the circulator, combined with a Green's function model, search methodology and appropriate search metrics. This approach significantly reduced the amount of real estate required for the integrated device, and reduced the copper losses associated with the use of open–circuit stub based impedance equalizers.

We have shown in the present work that impedance equalization may be accomplished by direct modification of the circulator material and geometrical parameters. One question that arises in connection with this work is whether other functionality can be accomplished by the circulator directly. For example, the circulator is shaped and fed similar to a circular microstrip patch antenna; can it be made to radiate in addition to circulate and provide impedance matching to a system? This possibility would enable significant reductions in real estate of phased array antennas for monostatic RADAR applications.

REFERENCES

[1] J. L. Young, R. S. Adams, B. O'Neil and C. M. Johnson, "Bandwidth Optimization of an Integrated Microstrip Circulator and Antenna Assembly: Part 1," *IEEE Antennas Propag. Mag.*, Vol. 48, No. 6, pp. 47–56, December 2006.

[2] J. L. Young and C. M. Johnson, "A Compact Recursive Trans–Impedance Green's Function for the Inhomogeneous Ferrite Microwave Circulator," *IEEE Trans. Microwave Theory Tech.*, vol. 52, No. 7, pp. 1751–1759, July 2004.

[3] N. Kaneda, W. R. Deal, Y. Qian, R. Waterhouse, and T. Itoh, "A broad–band planar quasi–Yagi antenna," *IEEE Trans. Ant. Propagat.*, vol. APS-50, no. 8, pp. 1158–1160, 2002.

Fig. 9. Simulation and measurement return loss of the system of Figure 6.

A Generalized Time–Stepping Algorithm for Electromagnetic Wave Propagation in Ferrite Media

Ryan S. Adams and Jeffrey L. Young

Abstract— A time integration scheme is considered herein for simulations of electromagnetic waves within a fully saturated ferrite medium. By considering Maxwell's equations in conjunction with the torque equation of motion for electron precession, we show that a stable second-order scheme can be achieved using both central differences and averages. The scheme is validated using a stripline phase shifter as a test case. Not only does the simulation agree quite well with results produced by a popular frequency-domain, finite element solver, the data also exhibits a very desirable, low-loss, phase shift effect.

Index Terms— Ferrites, Ferrite Phase Shifters, Magnetic Materials, FDTD.

I. INTRODUCTION

During the past decade there has been considerable research activity in the modeling of electromagnetic waves within a fully saturated ferrite using time-domain, Maxwellian field solvers. Two popular approaches have been considered to date – recursive convolution (RC) and direct integration (DI). The RC methods use the time-domain representation of the Polder terms of the susceptibility matrix in conjunction with the constitutive convolution integral as the governing equation for the ferrite. Depending on whether the convolution integral is discretized using piecewise constant or piecewise linear interpolation, Schuster and Luebbers [1] and others were able to achieve stable schemes that yielded first or second order solutions. Other researchers, such as [2] – [4], adopted various direct integration methods, whereby the dynamic torque equation of electron precession is used as the starting point. In these cases, one-sided differences, central differences and/or central averages are invoked to discretize the torque equation.

The scheme considered herein continues the development of the direct integration methodologies by following a similar line of thought advocated by [4]. However, instead of rewriting the torque equation in terms of the magnetic flux density B and the magnetic intensity H, as was done by [4], we opt to write the torque equation in terms of the magnetic flux density B and the magnetization M. By doing so, we leave the torque equation in its natural state variable form, which allows us then to discretize it using central differences and averages. The resulting discretized equation is couched in a compact form using dyadic and vector operations and is valid for any direction of ferrite bias field.

It has been our goal to follow the philosophy of developing FDTD schemes for dispersive media by adding equivalent magnetization terms to Faraday's law (as in the case of ferrites) or polarization terms to Ampere's law (as in the case of Debye [5], Lorentz [6] or plasma media [7]). By doing so, we never modify the core Yee algorithm, as expressed in terms of E and B in Faraday's law and H and D in Ampere's law, regardless of the media type considered. The scheme described herein achieves this goal.

To validate the proposed integration methodology, a three-dimensional, stripline phase shifter is considered in which the field bias is in the direction of propagation. This device is particularly attractive for our purposes, since various biasing fields need to be considered to see the phase shift effect. Using a solution produced by a frequency-domain, finite-element solver as a standard, we show near perfect agreement between that standard and the data produced by the proposed scheme. Moreover, from a device performance point of view, a full 180° phase shift can be observed by adjusting the effective internal field from 0 Oe to 2800 Oe; the return loss remains below 20 dB and the transmission loss remains below 0.5 dB over this same range. To validate that the proposed scheme can accomodate an arbitrary direction of magnetic bias, this geometry was again simulated using an obliquely directed bias direction; excellent correlation is again shown. As a final analysis of this device, a simulation was completed using 1,000,000 timesteps; no late–time stability problems were noted.

II. FORMULATION

Within the ferrite material, the magnetization M and magnetic intensity H are related to each other by the Gilbert equation of motion, including the phenomenological loss term [8]. This equation can be expressed as

$$\frac{\partial \mathbf{M}}{\partial t} = -\mu_\circ |\gamma| \mathbf{M} \times \mathbf{H} - \frac{\alpha}{|\mathbf{M}|} \mathbf{M} \times \frac{\partial \mathbf{M}}{\partial t}, \qquad (1)$$

where $\mu_\circ$ is the permeability of free space, $\gamma = 1.759 \times 10^{11}$ C/kg is the gyromagnetic ratio and α is a damping factor. The vectors M and H consist of both dc and ac components. The dc component of H is the total effective internal dc magnetic intensity; the dc component of M is the internal dc magnetization.

The ac magnetic flux density is related to the magnetic intensity and magnetization as [9]

$$\mathbf{H}_{ac} = \frac{1}{\mu_\circ} \mathbf{B}_{ac} - \mathbf{M}_{ac}, \qquad (2)$$

so the total magnetic intensity within the ferrite is given by

$$\mathbf{H} = \mathbf{H}_{dc} + \frac{1}{\mu_\circ} \mathbf{B}_{ac} - \mathbf{M}_{ac}. \qquad (3)$$

In this work we define a vector *Larmor* precession frequency $\bar{\omega}_\circ$ and vector magnetization frequency $\bar{\omega}_m$ such that

$$\bar{\omega}_\circ = \mu_\circ \gamma \mathbf{H}_{dc} = \omega_{\circ_x} \mathbf{a}_x + \omega_{\circ_y} \mathbf{a}_y + \omega_{\circ_z} \mathbf{a}_z \qquad (4)$$

and

$$\bar{\omega}_m = \mu_\circ \gamma \mathbf{M}_{dc} = \omega_{m_x} \mathbf{a}_x + \omega_{m_y} \mathbf{a}_y + \omega_{m_z} \mathbf{a}_z. \qquad (5)$$

Eqn. (1) can then be expressed as

$$\frac{\partial \mathbf{M}_{ac}}{\partial t} = -\mu_\circ \gamma \mathbf{M}_{dc} \times \mathbf{H}_{dc} - \mathbf{M}_{ac} \times (\overline{\omega}_m + \overline{\omega}_\circ)$$

$$+ \frac{1}{\mu_\circ} \mathbf{B}_{ac} \times \overline{\omega}_m - \gamma \mathbf{M}_{ac} \times \mathbf{B}_{ac}$$

$$+ \frac{\alpha}{|\overline{\omega}_m|} \frac{\partial \mathbf{M}_{ac}}{\partial t} \times \overline{\omega}_m - \frac{\alpha}{|\mathbf{M}|} \mathbf{M}_{ac} \times \frac{\partial \mathbf{M}_{ac}}{\partial t}. \quad (6)$$

If we assume that $|\mathbf{M}_{ac}| \ll |\mathbf{M}_{dc}|$, $|\mathbf{H}_{ac}| \ll |\mathbf{H}_{dc}|$, $\mathbf{M}_{dc}$ is parallel with $\mathbf{H}_{dc}$ and $|\mathbf{M}_{dc}| = M_s$, then Eqn. (6) becomes

$$\frac{\partial \mathbf{M}_{ac}}{\partial t} = \frac{1}{\mu_\circ} \mathbf{B}_{ac} \times \overline{\omega}_m - \mathbf{M}_{ac} \times (\overline{\omega}_m + \overline{\omega}_\circ) + \frac{\alpha}{|\overline{\omega}_m|} \frac{\partial \mathbf{M}_{ac}}{\partial t} \times \overline{\omega}_m. \quad (7)$$

In so far as the equation of motion given by Eqn. (1) is valid, Eqn. (7) represents the relationship between $\mathbf{M}$ and $\mathbf{B}$ within a fully saturated ferrite under small–signal conditions. This equation, as cast in terms of dc biasing fields and ac signal fields will be the basis for the subsequent discretization procedure. For the purposes herein, we will regard the Gilbert form of the Landau–Lifschitz model to be phenomenologically true in the form given by Eqn. (7) [10].

Along with Eqn. (7), the equations governing the electro-magnetic problem are:

$$\frac{\partial \mathbf{E}_{ac}}{\partial t} = \frac{1}{\epsilon} \nabla \times \mathbf{H}_{ac}, \quad (8)$$

$$\frac{\partial \mathbf{B}_{ac}}{\partial t} = -\nabla \times \mathbf{E}_{ac} \quad (9)$$

and Eqn (2), where $\mathbf{E}_{ac}$ is the ac electric intensity and $\mathbf{B}_{ac}$ is the ac magnetic flux density. These equations, along with Eqn. (7) can be temporally discretized using both central differences and averages as follows:

$$\mathbf{E}_{ac}^{n+1/2} = \mathbf{E}_{ac}^{n-1/2} + \frac{\delta_t}{\epsilon} \nabla \times \mathbf{H}_{ac}^n, \quad (10)$$

$$\mathbf{B}_{ac}^{n+1} = \mathbf{B}_{ac}^n - \delta_t \nabla \times \mathbf{E}_{ac}^{n+1/2}, \quad (11)$$

$$\mathbf{M}_{ac}^{n+1} = \mathbf{M}_{ac}^n + \frac{\delta_t}{\mu_\circ} \left(\frac{\mathbf{B}_{ac}^{n+1} + \mathbf{B}_{ac}^n}{2} \right) \times \overline{\omega}_m$$

$$- \delta_t \left(\frac{\mathbf{M}_{ac}^{n+1} + \mathbf{M}_{ac}^n}{2} \right) \times (\overline{\omega}_m + \overline{\omega}_\circ)$$

$$+ \frac{\alpha}{|\overline{\omega}_m|} \left(\mathbf{M}_{ac}^{n+1} - \mathbf{M}_{ac}^n \right) \times \overline{\omega}_m, \quad (12)$$

$$\mathbf{H}_{ac}^{n+1} = \frac{1}{\mu_\circ} \mathbf{B}_{ac}^{n+1} - \mathbf{M}_{ac}^{n+1}. \quad (13)$$

It should be noted that $\mathbf{M}_{ac}, \mathbf{H}_{ac}$ and $\mathbf{B}_{ac}$ are all temporally synchronized in the aforementioned scheme. Equations (10) – (13) are valid for any numerical scheme that employs both temporal central differences and averages.

To obtain an implementation algorithm associated with Eqn. (12), we must first solve for $\mathbf{M}_{ac}^{n+1}$. To do this, we define the following dyads couched in matrix form:

$$\overline{\overline{\omega}}_m = \begin{bmatrix} 0 & \omega_{m_z} & -\omega_{m_y} \\ -\omega_{m_z} & 0 & \omega_{m_x} \\ \omega_{m_y} & -\omega_{m_x} & 0 \end{bmatrix}, \quad (14)$$

$$\overline{\overline{M}}_1 = \begin{bmatrix} 1 & M_{1_z} & -M_{1_y} \\ -M_{1_z} & 1 & M_{1_x} \\ M_{1_y} & -M_{1_x} & 1 \end{bmatrix} \quad (15)$$

and

$$\overline{\overline{M}}_2 = \begin{bmatrix} 1 & M_{2_z} & -M_{2_y} \\ -M_{2_z} & 1 & M_{2_x} \\ M_{2_y} & -M_{2_x} & 1 \end{bmatrix}. \quad (16)$$

The elements of $\overline{\overline{M}}_1$ and $\overline{\overline{M}}_2$ are given by

$$M_{1_n} = \frac{\delta_t}{2} (\omega_{m_n} + \omega_{o_n}) - \frac{\alpha \omega_{m_n}}{|\overline{\omega}_m|}, \quad n = x, y, z \quad (17)$$

and

$$M_{2_n} = -\frac{\delta_t}{2} (\omega_{m_n} + \omega_{o_n}) - \frac{\alpha \omega_{m_n}}{|\overline{\omega}_m|}, \quad n = x, y, z. \quad (18)$$

With these definitions, Eqn. (12) can be expressed as

$$\mathbf{M}_{ac}^{n+1} = \overline{\overline{M}}_1^{-1} \cdot \overline{\overline{M}}_2 \cdot \mathbf{M}_{ac}^n + \frac{\delta_t}{2\mu_\circ} \overline{\overline{M}}_1^{-1} \cdot \overline{\overline{\omega}}_m \cdot \left(\mathbf{B}_{ac}^{n+1} + \mathbf{B}_{ac}^n \right), \quad (19)$$

where, for example, $\overline{\overline{M}}_2 \cdot \mathbf{M}_{ac}^n$ represents a dyadic–vector dot product operation.

To complete our treatment, we choose to employ the Yee cell of Figure 1 in conjunction with spatial central differences and averages. With this cell arrangement, Eqns. (10) - (11) can be spatially discretized as in the traditional Yee scheme [11]. Since the components of the magnetization vector have been placed coincident with the magnetic flux density and magnetic intensity, Eqn. (13) requires no spatial averaging. With the grid chosen according to Figure 1, Eqn. (19) shows that M_x^{n+1} depends on the previous values of M_y^n, M_z^n, $B_y^{n+1/2}$ and $B_z^{n+1/2}$, each of which is not located at the same point in the grid as M_x^{n+1}. Hence, each of these components require four–point spatial averaging to compute the correct value at the location of M_x within the grid. Similar statements can be made about four–point spatial averaging for the update equations for M_y^{n+1} and M_z^{n+1}.
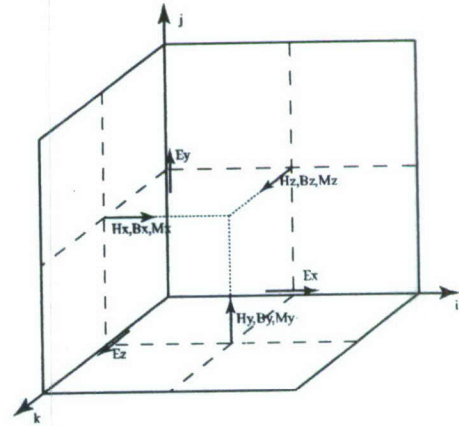

Fig. 1. Yee grid cell for this new scheme.

III. RESULTS

Consider the stripline phase shifter topology shown in Figure 2. This problem is an appealing validation geometry for the algorithm presented herein, as it provides a mixture of different materials (substrate, PEC and ferrite), allows a

comparison of several different values of effective internal field and requires an applied bias in a direction different from bias normal to the plane of the circuit.

The geometrical parameters chosen for this validation are $W_f = 2.9$mm, $L_f = 24$mm, $W = 1.1$mm and $h = 2$mm; the width of the domain is 8.6mm. The ferrite material chosen is Trans–Tech TTVG-1000 which has a dielectric constant of $\epsilon_f = 14$, magnetic saturation $4\pi M_s = 1000$ G and linewidth $\Delta H = 10$ Oe, as measured at $f_{meas} = 9.4$GHz. The surrounding material is Trans–Tech D-16 Mg-Ti which has a dielectric constant of $\epsilon_d = 16$. From these parameters, $\omega_m = \mu_o \gamma M_s = 1.76 \times 10^{10}$ rad/s and $\alpha = \mu_o \gamma \Delta H / 2\omega_{meas} = 0.237 \times 10^{-4}$. The width of the trace is set to achieve a 25Ω characteristic impedance.
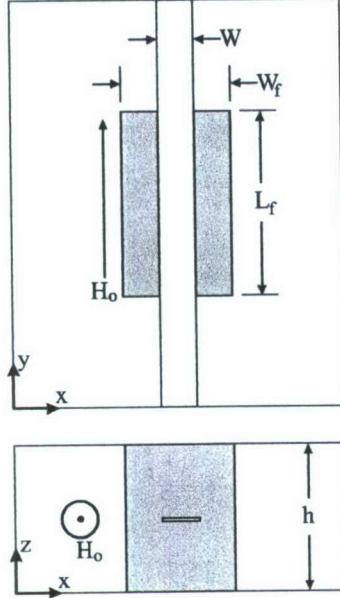

Fig. 2. Stripline phase shifter validation topology. The darker shaded region represents the ferrite.

The stripline's TEM waves are excited and detected per the method described in [12]. This approach allows for a much smaller domain size than would otherwise be required as the source and terminal planes of the simulation can be placed arbitrarily near the ferrite/dielectric interface without loss of accuracy. The pulse chosen to characterize the circuit is gaussian of width a, where $a = 6.065 \times 10^{10}$ 1/s; the pulse is of the form e^{-t^2/a^2}.

To determine appropriate cell size, we must first consider the wavelength within the ferrite material. Per [10], $\lambda = 2\pi/k$ and $k = \omega\sqrt{\mu_e \epsilon}$, where $\mu_e = (\mu_f^2 - \kappa^2)/\mu_f$, and

$$\mu_f = \mu_o \left(1 + \frac{\omega_o \omega_m}{\omega_o^2 - \omega^2} \right), \tag{20}$$

$$\kappa = \mu_o \frac{\omega \omega_m}{\omega_o^2 - \omega^2}. \tag{21}$$

At an operating frequency of 13 GHz, $\lambda = 6.3$mm for an effective internal field of zero, and $\lambda = 8.1$mm for an effective internal field of 3000 Oe. To achieve superb accuracy, the cell size is chosen to be less than $\lambda/40$ which for the shortest

wavelength is 0.158mm. For convenience in accomodating the correct dimensions described previously, the following cell dimensions were chosen: $\delta_x = 0.15$mm, $\delta_y = 0.1$mm and $\delta_z = 0.1$mm. The overall domain size was chosen to be 100 cells in the y–direction, 180 cells in the x–direction and 20 cells in the z–direction. The timestep was chosen utilizing a CFL stability criteria of 0.5 so that $\delta_t \approx 0.1$ ps.

To validate the algorithm presented herein, a comparison of the real and imaginary transmitted scattering parameters of the phase shifter was made with Ansoft's High Frequency Structure Simulator (HFSS), as shown in Figure 3. In this plot, we see very good correlation between the two data sets, thus indicating that for the fully saturated and low power case, the algorithm is consistent with frequency–domain formulations.
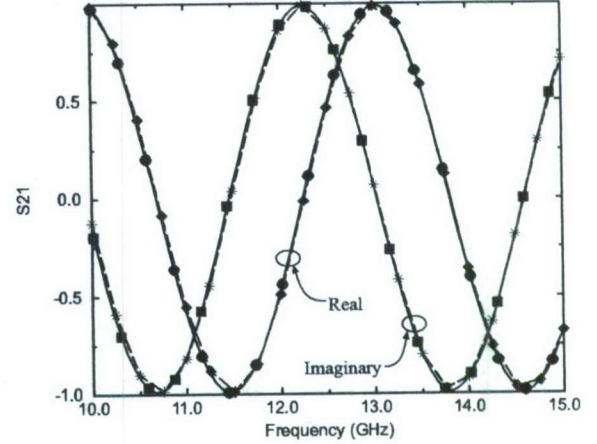

Fig. 3. A comparison of S_{21} with HFSS for effective internal field equal to zero. Solid lines are FDTD and dashed lines are HFSS.

The simulated return loss of this device at 13 GHz is shown in Figure 4. This plot indicates that the device is usable in a 25Ω system with better than 20dB specification for an effective internal field less than 2900 Oe. The simulated phase shift at 13 GHz is shown in Figure 5 and shows that for a reasonable effective internal field strength, this device can realize greater than $180°$ phase shift.
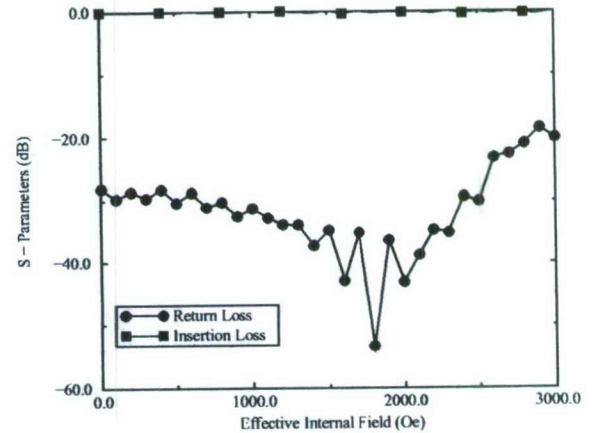

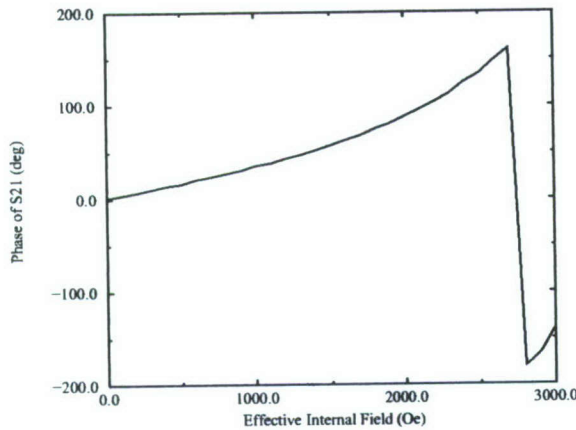Fig. 4. Return loss of the device as a function of applied field when $f = 13$ GHz.

Fig. 5. Phase shift of the device as a function of applied field when $f = 13$ GHz.

Fig. 6. A comparison of S_{21} with HFSS for an oblique bias direction and effective internal field equal to zero. Solid lines are FDTD and dashed lines are HFSS.

To achieve variation in the effective internal field as shown in Figs 4 and 5, variation of the externally applied bias is necessary. To determine what the appropriate external field should be, we assume a homogeneous ferrite, in which case, $H_{int} = H_{applied} - (4\pi M_s N_{yy})$, where N_{yy} is the demagnetization factor. Due to the geometrical shape of the ferrite material, the demagnetizing factor, as given by Joseph and Schlömann [13], is approximately zero, hence the effective internal field is equal to the externally applied bias.

One of the significant contributions of the proposed scheme is its ability to model ferrites whose bias direction points in a direction different from the cartesian coordinate axes. To validate this capability, the simulation parameters above were used with a ferrite having an oblique bias direction and an internal field of zero. The bias was chosen to have the following direction cosines: $\cos\alpha = 0.54$, $\cos\beta = 0.31$ and $\cos\gamma = 0.78$, where α is measured from the x–axis, β from the y–axis and γ from the z–axis. A comparison of the real and imaginary transmitted scattering parameters of the device as determined from the proposed scheme and HFSS is shown in Figure 6. As before, this plot shows very good correlation between the two data sets. As an additional validation of the proposed scheme, this simulation was accomplished with 1,000,000 timesteps to examine late–time stability; no late–time stability problems were noted.

IV. CONCLUSION

A highly efficient time-domain scheme has been presented for the simulation of electromagnetic waves within ferrite media. In this investigation, we limited our treatment to electromagnetic modes of low wavenumbers. However, for very large wavenumbers (i.e. $k > 10$ r/cm), it is well known that electric intensity becomes small enough to be neglected. The magnetic intensity, however, becomes irrotational and the mode that propagates is regarded as magnetostatic. For even larger wavenumbers (i.e., $k > 10^5$ r/cm), a spin wave can be supported in the ferrite. Due to these large wavenumbers, it is questionable whether the explicit scheme presented herein is satisfactory, due to the limitations of the CFL number. (This problem was also noted in [7] with respect to the simulation
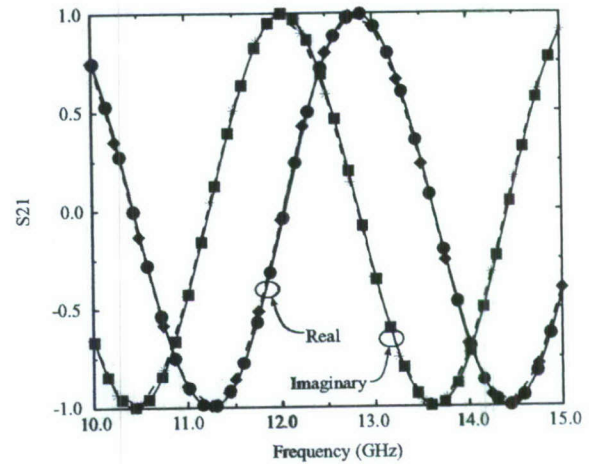
of waves in warm plasmas. In that case, the large disparities in wavenumbers between the optical and acoustic modes created algorithmic difficulties.) Future work in this area is clearly needed.

REFERENCES

[1] J. W. Schuster and R. J. Luebbers, "Finite difference time domain analysis of arbitrarily biased magnetized ferrites," *Radio Sci.*, vol. 31, no. 4, pp. 923–930, Jul–Aug 1996.

[2] G. Zheng and K. Chen, "Transient analysis of microstrip lines with ferrite substrate by extended FD-TD method," *Int. J. Infrared & Millimeter Waves*, vol. 13, No. 8, pp. 1115–1125, 1992.

[3] M. Okoniewski and E. Okoniewska, "FDTD analysis of magnetized ferrites: a more efficient algorithm," *IEEE Microwave Guided Wave Lett.*, vol. 4, No. 6, pp. 169–171, June 1994.

[4] J. A. Pereda, L. A. Vielva, M. A. Solano, A. Vegas and A. Prieto, "FDTD analysis of magnetized ferrites: application to the calculation of dispersion characteristics of ferrite–loaded waveguides," *IEEE Trans. Microwave Theory Tech.*, vol. MTT-43, no. 2, pp. 350–357, Feb 1995.

[5] J. L. Young and R. S. Adams, "On the time integration of Maxwells equations associated with Debye relaxation processes," *IEEE Trans. Ant. Propagat.*, Vol. 55, No. 8, pp. 2409–2412, Aug 2007.

[6] J.L. Young, "Propagation in linear dispersive media: Finite difference time-domain methodologies," *IEEE Trans. Ant. Propagat.*, vol. 43, no. 4, pp. 422-426, 1995.

[7] J. L. Young, "A full FDTD implementation for radio wave propagation in a plasma," *Radio Sci.*, vol. 29, no. 6, pp. 1513–1522, 1994.

[8] T. L. Gilbert,"A Phenomenological theory of damping in ferromagnetic materials." *IEEE Trans. Magn.*, Vol. 40, No. 6, pp. 3443 – 3449, Nov. 2004.

[9] D. M. Pozar, *Microwave Engineering*, 2nd. Ed., Wiley, New York, NY, 1998.

[10] B. Lax and K. J. Button, *Microwave Ferrites and Ferrimagnetics*, McGraw–Hill, New York, NY, 1962.

[11] K. S. Yee, "Numerical solution of initial boundary value problems involving Maxwell's equations in isotropic media," *IEEE Trans. Ant. Propagat.*, vol. AP-14, Issue 3, pp. 302–307, 1966.

[12] J. L. Young and R. Adams, "Excitation and detection of waves in the FDTD analysis of N–Port networks." *Progress in Electromagnetic Research*, vol. 53, pp. 249–269, 2005.

[13] R. I. Joseph and E. Schlömann, "Demagnetizing field in nonellipsoidal bodies," *J. Appl. Phys.*, vol. 36, no. 5, pp. 1579–1593, 1965.